U.S. DEPARTMENT OF COMMERCE
National Technical Information Service
PB-292 751

Optical Instrument for In-Stack Monitoring of Particle Size

Leeds and Northrup Co, North Wales, PA

Prepared for

Environmental Sciences Research Lab, Research Triangle Park, NC

Feb 79

United States
Environmental Protection
Agency

Environmental Sciences Research
Laboratory
Research Triangle Park NC 27711

EPA-600/2-79-032
February 1979

PB 292751

Research and Development

EPA

Optical Instrument for In-Stack Monitoring of Particle Size

REPRODUCED BY
NATIONAL TECHNICAL
INFORMATION SERVICE
U. S. DEPARTMENT OF COMMERCE
SPRINGFIELD, VA. 22161

RESEARCH REPORTING SERIES

Research reports of the Office of Research and Development, U.S. Environmental Protection Agency, have been grouped into nine series. These nine broad categories were established to facilitate further development and application of environmental technology. Elimination of traditional grouping was consciously planned to foster technology transfer and a maximum interface in related fields. The nine series are:

1. Environmental Health Effects Research
2. Environmental Protection Technology
3. Ecological Research
4. Environmental Monitoring
5. Socioeconomic Environmental Studies
6. Scientific and Technical Assessment Reports (STAR)
7. Interagency Energy-Environment Research and Development
8. "Special" Reports
9. Miscellaneous Reports

This report has been assigned to the ENVIRONMENTAL PROTECTION TECHNOLOGY series. This series describes research performed to develop and demonstrate instrumentation, equipment, and methodology to repair or prevent environmental degradation from point and non-point sources of pollution. This work provides the new or improved technology required for the control and treatment of pollution sources to meet environmental quality standards.

This document is available to the public through the National Technical Information Service, Springfield, Virginia 22161.

TECHNICAL REPORT DATA
(Please read Instructions on the reverse before completing)

1. REPORT NO. EPA-600/2-79-032	2.
3. RECIPIENT'S ACCESSION NO. PB292751	
4. TITLE AND SUBTITLE: OPTICAL INSTRUMENT FOR IN-STACK MONITORING OF PARTICLE SIZE	5. REPORT DATE: February 1979
	6. PERFORMING ORGANIZATION CODE
7. AUTHOR(S): A.L. Wertheimer and M.N. Trainer	8. PERFORMING ORGANIZATION REPORT NO.
9. PERFORMING ORGANIZATION NAME AND ADDRESS: Leeds & Northrup Company, Dickerson Road, North Wales, Pennsylvania 19454	10. PROGRAM ELEMENT NO. 1AD712 BC-11 (FY-78)
	11. CONTRACT/GRANT NO. 68-02-2447
12. SPONSORING AGENCY NAME AND ADDRESS: Environmental Sciences Research Laboratory-RTP,NC, Office of Research and Development, U.S. Environmental Protection Agency, Research Triangle Park, N.C. 27711	13. TYPE OF REPORT AND PERIOD COVERED: Final 10/76-10/78
	14. SPONSORING AGENCY CODE: EPA/600/09
15. SUPPLEMENTARY NOTES	

16. ABSTRACT

A new light scattering instrument for in-situ measurements of particulates in the 0.2 to 10.0 micron diameter size range is described. Two modes of scattering are used, each with two wavelengths of light, to generate five size fractions by volume from a distribution of particulates. One mode measures polarized light scattered in two orthogonal orientations at an angle of 90° to the optical probe beam. The second mode measures light scattered in near forward angles (4 to 11°). Both modes allow the extraction of size data when particles of different sizes are present simultaneously in the sensing region. These principles have been incorporated into a prototype portable stack monitor, consisting of a 1.5 meter long, 9 cm diameter insertable probe capable of withstanding temperatures up to 260°C. The optical signals are carried through fiber optic cables contained in the probe. An arc source and silicon photodetectors are outside the stack at the end of the probe, while a digital microprocessor analyzes the set of measurements and calculates the size fractions. The microprocessor, an air purge system, the lamp power supply, and a digital printer are housed separately from the probe for ease of installation and service.

The completed instrument was tested on coal-fired fly ash particulates in the laboratory at a stationary source simulator facility and in the field at a coal-fired power plant. Results and comparisons with other sizing techniques are presented.

17. KEY WORDS AND DOCUMENT ANALYSIS

a. DESCRIPTORS	b. IDENTIFIERS/OPEN ENDED TERMS	c. COSATI Field/Group
*Air pollution *Particles *Particle size distribution *Monitors *Optical equipment Flue gases Evaluation		13B 20F 21B

18. DISTRIBUTION STATEMENT: RELEASE TO PUBLIC	19. SECURITY CLASS (This Report): UNCLASSIFIED	21. NO. OF PAGES: 78
	20. SECURITY CLASS (This page): UNCLASSIFIED	22. PRICE: PC A05/MF A01

EPA Form 2220-1 (Rev. 4-77) PREVIOUS EDITION IS OBSOLETE

EPA-600/2-79-032
February 1979

OPTICAL INSTRUMENT FOR IN-STACK MONITORING OF PARTICLE SIZE

by

A.L. Wertheimer
M.N. Trainer
Leeds & Northrup Company
North Wales, Pa. 19454

Contract No. 68-02-2447

Project Officer

William D. Conner
Emission Measurement and Characterization Division
Environmental Sciences Research Laboratory
Research Triangle Park, North Carolina 27711

ENVIRONMENTAL SCIENCES RESEARCH LABORATORY
OFFICE OF RESEARCH AND DEVELOPMENT
U.S. ENVIRONMENTAL PROTECTION AGENCY
RESEARCH TRIANGLE PARK, NORTH CAROLINA 27711

DISCLAIMER

This report has been reviewed by the Environmental Sciences Research Laboratory, U.S. Environmental Protection Agency, and approved for publication. Approval does not signify that the contents necessarily reflect the views and policies of the U.S. Environmental Protection Agency, nor does mention of trade names or commercial products constitute endorsement or recommendation for use.

ABSTRACT

A new light scattering instrument for in-situ measurements of particulates in the 0.2 to 10.0 micron diameter size range is described. Two modes of scattering are used, each with two wavelengths of light, to generate five size fractions by volume from a distribution of particulates. One mode measures polarized light scattered in two orthogonal orientations at an angle of 90° to the optical probe beam. The second mode measures light scattered in near forward angles (4 to 11°). Both modes allow the extraction of size data when particles of different sizes are present simultaneously in the sensing region. These principles have been incorporated into a prototype portable stack monitor, consisting of a 1.5 meter long, 9 cm diameter insertable probe capable of withstanding temperatures up to 260°C. The optical signals are carried through fiber optic cables contained in the probe. An arc source and silicon photodetectors are outside the stack at the end of the probe, while a digital microprocessor analyzes the set of measurements and calculates the size fractions. The microprocessor, an air purge system, the lamp power supply, and a digital printer are housed separately from the probe for ease of installation and service.

The completed instrument was tested on coal-fired fly ash particulates in the laboratory at a stationary source simulator facility and in the field at a coal-fired power plant. Results and comparisons with other sizing techniques are presented.

This report was submitted in fulfillment of Contract 68-02-2447 by Leeds and Northrup Company under the sponsorship of the U.S. Environmental Protection Agency. This report covers a period from October 1976 to October 1978.

CONTENTS

Figures vi
Tables viii
Acknowledgements ix

1. Introduction 1
2. Conclusions and Recommendations. 2
3. Optical Research Activities 4

Theory 4

Additional Theory & Experiments on 90° Scattering . . 10

Refinements of the 90° Scattering Response . 15

Signal Level Computations 18

Studies of Alternate Configurations. . . . 19

4. Theory of Instrument Design 25

Operating Environment 25

Optical Design. 25

Spectral Balance 26

Electronic Filter. 27

Purge System 28

Air Curtains 30

Summary Description 32

5. Testing of the Prototype 35

Theoretical Calibrations 35

In-house Calibration of the Completed Unit . 43

Field Trial at EPA Facility 53

Field Trial at a Coal-Fired Facility . . . 58

Modifications During System Testing. . . . 61

6. Conclusions 63

References 66

FIGURES

Number		Page
1.	Log of scattered intensity per particle as a function of observation angle, with forward direction at 180°. (Two orthogonal polarizations of incident light are shown.) . . .	5
2.	Intensity difference per unit volume, $(I_1 - I_2)/a^3$, for a scattering angle of 90°	6
3.	Configurations for 90° scattering for polarizations of light.	8
4.	Experiment & theory for polystyrene spheres in water, n = 1.20	9
5.	Spectrophotofluorometer system used for experimental data in Figure 4	10
6.	Volume response for different collection angles around 90°. .	11
7.	Volume response at 90° for index = 1.96 - 0i	12
8.	Volume response at 90° for index = 1.96 - 0.66i (absorptive flyash)	12
9.	Schematic drawing of laboratory system used to verify the volumetric response functions for 90° scattering.	13
10.	Experiments using system in Figure 9, with polystyrene spheres in water	14
11.	Theoretical and experimental curves for 90° scattering using absorbing and transparent material, showing the flux difference $i_2 - i_2$, per unit volume of material. Two sizes of polystyrene spheres were used, 0.234 and 0.801 microns in diameter, and the wavelength was varied to change the size parameter, a . . .	15
12.	Comparison of different weightings of the difference, I_1-KI_2 .	16
13.	Effect of broadening the spectral bandwidth	17

Number		Page
14.	Integral of primary peak as a function of real and complex portions of refractive index.	18
15.	Stack and remote configurations for particulate size monitor, as originally proposed.	19
16.	90° scatter system with forward scattering capabilities.	21
17.	Background/main beam ratio vs. scatter angle	24
18.	Schematic drawing of optical system	27
19.	Schematic drawing of electronic filter circuit.	29
20.	Schematic drawing of blower and pneumatic components.	29
21.	Basic air curtain design and gas flow.	31
22.	Air chamber and an additional orifice plate used to create serial mixing chambers.	31
23.	Air chamber with baffle to confine and direct air flow	32
24.	Photograph of stack probe including all components	34
25.	Comparison of forward scattering common volumes with and without water in cell	44
26.	Flux/Unit volume vs. particle diameter for DOP, Aerosols, λ = 0.45 microns.	46
27.	Flux/Unit volume vs. particle size for DOP, Aerosols, λ = 0.09.	46
28.	Laboratory sample system for delivery of aerosol smokes.	47
29.	Volumetric histograms of several smokes	51
30.	Volumetric histograms for various dioctylphthalate concentrations and for cigar smoke.	52
31.	Size of fly ash as measured by impactor and optical monitor at EPA, RTP source simulator.	56
32.	Volumetric response curves, as a function of particle diameter, for the five channels of the prototype. Curves 1 and 2 are obtained with 90° scattering, and curves 3, 4, and 5 from forward scattering. These curves are for silica, with refractive index of 1.5.	63
33.	Probe, electronics package, and digital printer used for measuring the size particulate material in utility stacks	64

TABLES

Number		Page
1.	Volume Response as a Function of Wavelength	7
2.	Background Normalized to Input Beam.	22
3.	Sample Region Purged with Dry Nitrogen.	23
4.	Histogram Intervals for Prototype Instrument.	36
5.	Forward Channels	37
6.	Symbol Definitions	37
7.	Volume and Transmission Factors	38
8.	Watts of Radiant Power for 1 Part/Billion per Channel	39
9.	Terms Used in 90° Calculations	40
10.	90° Signals for 1 Part/Billion	41
11.	Detector Gains.	42
12.	Preliminary Channel Equations.	42
13.	Normalized Response for Each Zone and the Inverse Matrix Used for Decoupling	43
14.	Theoretically Predicted Ratios for Three Particle Sizes	49
15.	Experimental Data with Various Aerosols	49
16.	Final Constants for the Prototype, as Built	50
17.	Fly Ash Sample Tests at EPA-RTP Source Simulator-May, 1978	54
18.	Impactor and Optical Volume Histograms for May, 1978 EPA/RTP Tests.	57
19.	Test Conditions	59
20.	Field Test Data from Coal Fired Facility	60
21.	Characteristics of Prototype Light Scattering Instrument.	65

ACKNOWLEDGMENTS

We wish to recognize the contributions of the following members of the Leeds and Northrup staff to the design and development program described in this report: Mr. Joe Haran, Mr. Howard Hart, Dr. Emil C. Muly, Mr. Ernest VanValkenburg and Dr. Hal Weber (Penn State University).

In addition, the EPA Technical Project Officer, Mr. William Conner, provided considerable help and guidance throughout this program and his assistance is gratefully acknowledged.

SECTION 1

INTRODUCTION

The purpose of this project was to develop a method for the real-time measurement of the size of particles in source emissions and to build a prototype instrument to verify performance of the methodology. The particle size range of interest is 0.2 to 10.0 microns, and the method of measurement of these particles is based on principles of light scattering. Two modes of scattering are used: near forward angle for the larger particles and 90^{o} scattering for the smaller sizes.

Prior to the start of the contract work, research on the methodology had been performed on determining volumetric fractions from the difference in 90^{o} scattered intensities of two orthogonally polarized beams. This approach formed the basis for the work described here.

The work plan for this project included two phases. The first was an experimental and laboratory demonstration phase, and the second involved the design, construction and evaluation of an on-stack instrument for measuring the size of particles of in-stack source emissions.

SECTION 2

SUMMARY - CONCLUSIONS AND RECOMMENDATIONS

A prototype optical light scattering instrument for measuring the size of particulate material in stacks has been designed, constructed, and tested. The prototype combines two optical scattering modes into a single instrument package for real-time measurement of volumetric fractions, according to size, in the respirable range of 0.1 to 10 microns in diameter. The application to stack analysis is unique and relatively new. Accordingly there is need for continuing development and analysis. This section provides a summary of the contract efforts, and the second section describes some recommendations for future work in this area.

Optical techniques involving low angle forward and polarization dependent 90° scattering have been combined in an instrument package for real-time particulate sizing in stationary sources. A significant extension to the technology of light scattering was the development and verification of the technique to measure volume fractions of sub-micron material. The concept involved measuring intensity differences of scattered, polarized light at 90° to the direction of a probe beam. This technique was engineered into a probe type configuration and combined with forward light scattering to provide five size fractions in the 0.1 to 10 micron diameter range.

An insertable probe was fabricated, designed and engineered for use in high temperature acid environments. Associated equipment; an air purge system and sophisticated electronics detection and microprocessor package, was designed and constructed.

Upon completion of the prototype, considerable effort was spent on insuring the calibration by the use of various aerosol materials. Field tests were conducted at EPA and at an East Coast coal-fired facility, and the results were compared with impactors. The unit was subsequently delivered to EPA for their use and evaluation.

The instrument offers a method for in-stack analysis of particle size without dilution or extraction of material, and directly produces a distribution of the particulates by volume fraction. This device thus provides a unique and valuable measurement capability for analysis and monitoring of particulates in source emissions.

RECOMMENDATIONS FOR FUTURE WORK

The principles of light scattering for particle size measurement have been well established. The forward scattering techniques are currently being applied in a range of particle sizing instruments, and the 90° scattering principles were verified carefully before and during the contract work.

The combination of the two techniques in a configuration suitable for stack particulate analysis produced a number of trade-off and compromise situations. Many of these trade-offs could not be fully evaluated until after the prototype was built and tested. While the unit works satisfactorily, our experience suggests that a number of items might be appropriate for future work. Some of these are listed here.

1. The arc lamp light source is ideal for some of its optical properties, such as its point source nature and broad spectral band width. However, some of the associated electrical difficulties, the starting pulse, in particular, required extensive circuit protection. With that in mind, a review of light sources for subsequent units would be in order.

2. The forward scattering configuration proved to be very difficult to calibrate, since each scattering angle covered a different region of the probe. Forward scattering subsequently became much more important for analysis of flyash samples than originally anticipated, as a significant fraction of the material was one micron or larger. A review of the forward scattering implementation would be appropriate for subsequent instrumentation.

3. The upper size limit could be extended in connection with the review in item 2, since forward scattering, in principle, is useful to sizes much greater than 10 microns.

4. Additional calibration experiments might be appropriate to verify the relationship between forward and 90° channels. Such experimentation would require a sophisticated particle or aerosol generation system to provide true Rayleigh scatterers, 0.1 microns in diameter or less, with sufficient number to provide a good optical signal. Our experience with conventional aerosols is that there is great difficulty in generating a high percentage of the mass of material below 0.5 microns.

SECTION 3

OPTICAL RESEARCH ACTIVITIES

Work under the contract began by measuring the optical flux scattered by polystyrene spheres from the submicron range to a few microns in diameter. These particles were illuminated by visible and near infrared sources and the scattered flux was analyzed as functions of wavelength, polarization, angular distribution, refractive index and absorption. Particular attention was given to the 90° observation angle since we had previously verified that size dependent information exists in the scatter flux at that angle.

A means was then developed to demonstrate in the laboratory the real-time measurement of particulate size, and equipment was assembled to demonstrate the feasibility of this method. During this process, forward angle light scattering was proposed and investigated as a practical alternative to measuring the portion of the particle size range which required long infrared wavelengths when using 90° scattering.

The Phase I effort was concluded by developing preliminary optical designs for the on-stack instrument which became the basis for the design specifications of the prototype instrument to be developed in Phase II. Inputs from the Project Officer concerning design and performance of the prototype were incorporated into the design.

THEORY

Considerable work was done on collecting measurements of particles in the 0.2 to 10 micron size range prior to September 27, 1976, when the contract began. This work was based on a new approach involving polarized light to determine volume fractions of material in well defined size ranges. The theoretical background to that approach is presented here.

For visible light, optical scattering characteristics for the majority of the particle size range of 0.2 to 10 microns must be determined through rigorous theory, referred to as Mie Scattering Theory.[1] Here, the exact size of the particle plays an important role. For spherical particles, the wavelength is usually expressed through the dimensionless quantity, $a = \pi d/\lambda$, with d as the diameter of the particle and λ as the wavelength. Within this realm, other parameters figure significantly in the characterization of scattering. The refractive index (both real and complex portions) influences the angular distribution of flux. The size and shape of the particle, as well as the polarization of the incident light, determines the pattern.

Mie theory has been studied by many researchers[2,3], and numerous tables of the angular distribution of flux have been prepared by others for use with problems of this nature. In order to illustrate some characteristics of the angular distribution of flux, Figure 1 presents graphs of the tabulated data[4] from a = 0.5 to 40 for spherical particles with an index of 1.33. Two orthogonal polarizations are shown, referred to as I_1 and I_2.

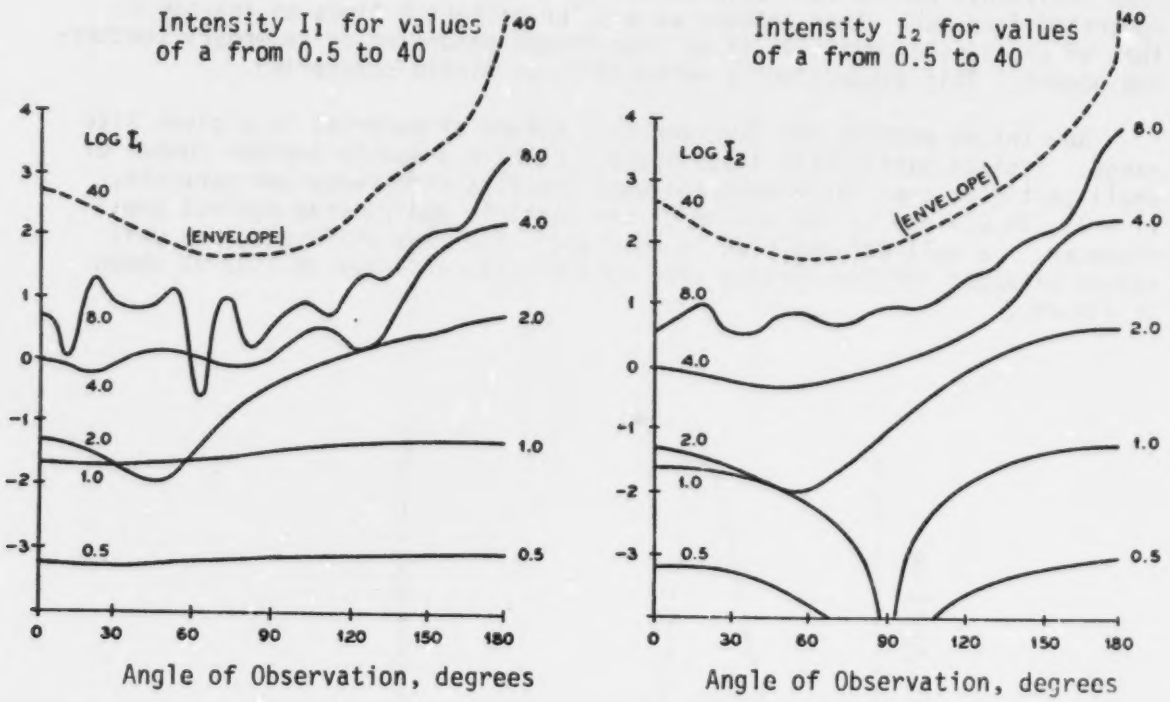

Figure 1. Log of scattered intensity per particle as a function of observation angle, with forward direction at 180°.
(Two orthogonal polarizations of incident light are shown.)

The log of the flux per particle is graphed, covering a hemisphere from 0° (light returning directly toward the source) through 180° (forward scattering direction). For a = 0.5 and 1.0, the Rayleigh scattering characteristics are evident, while for a = 40, only the envelope of the pattern is shown; the flux is mostly in the forward direction. These curves change somewhat as the refractive index is varied. However, one of the most stable characteristics of the patterns for different indices of refraction is the null at 90° for small values of "a" with I_2, that is, for light polarized so that the electric field is in the plane defined by the direction of propa-

gation of the incident beam and the point of observation.

The difference in intensity can be calculated by subtracting the two curves at 90°. The percentage change is greatest for a = 0.5 and 1.0, since I_2 goes to zero at 90°. However, the absolute value of the difference per particle generally increases as the diameter increases.

It should be mentioned that these curves describe the light scattered from individual particles. Suspensions of N identical particles widely separated from each other produce an angular pattern N times as intense as that of the single particle, if no significant shadowing or secondary scattering occurs. This assumption is referred to as single scattering.

Now let us examine the flux per unit volume of material in a given size range. Typical particulate distributions contain a vastly greater number of small particles than large ones and when the flux difference per particle, $I_1 - I_2$, is divided by the volume of the particle and plotted against the diameter, a well-defined peak is observed. The flux difference per unit volume at about 90° for various size spheres with an index of 1.33 is shown in Figure 2.

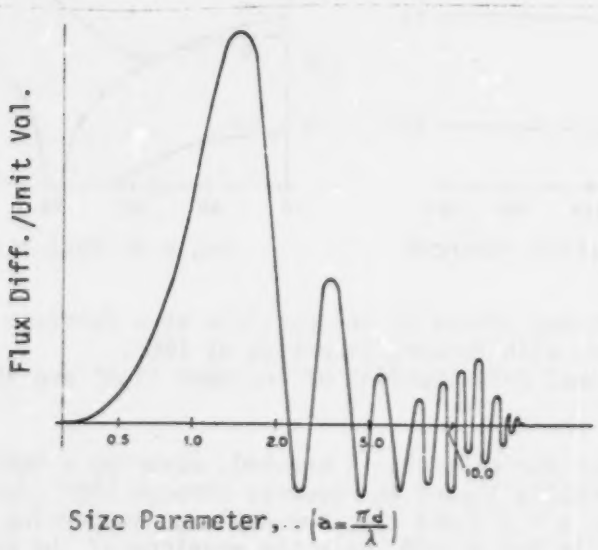

Figure 2. Intensity difference per unit volume, $(I_1 - I_2)/a^3$, for a scattering angle of 90°.

This curve has a peak at about a = 1.5, and the half width covers approximately a range from a = 1 to 2. In order to identify a corresponding particle size, a wavelength must be specified. For a helium-neon laser, with λ = 0.6328 microns, the half width covers diameters from .2 to .4 microns, and the peak is located at 0.3 microns. Based on this response curve, other wavelengths can be used to measure volume components at other size ranges, as shown in Table 1.

The curve in Figure 2 is for a specific refractive index, 1.33. Other indices produce slightly different curves, although the basic characteristics are preserved. The curve for glass spheres, for example (n = 1.55) has its peak at approximately the same value (a = 1.5) and is quite similar in shape to the curve in Figure 2 for the region around a = 1.5. The differences occur principally in the fine structure to the right of the first peak.

TABLE 1. VOLUME RESPONSE AS A FUNCTION OF WAVELENGTH

(*Fundamental Laser Wavelengths)

Wavelength	Particle Diameter at Peak of Response	50% Range
0.4 microns	0.2 microns	.13 to .25 microns
0.6328 microns*	0.3 microns	.20 to .40 microns
1.06 microns*	0.5 microns	.34 to .67 microns
1.25 microns	0.6 microns	.40 to .80 microns
2.2 microns	1.05 microns	.70 to 1.4 microns
10.6 microns*	5.06 microns	3.4 to 6.7 microns
11.6 microns	5.5 microns	3.7 to 7.4 microns

Figure 3 shows the basic scattering configurations for measurement of intensities, I_1 and I_2, for two orthogonal polarizations of light. I_1 and I_2 are related to the tabulated Mie scattering functions, i_1 and i_2, through the following equations:

$$I_1 = I_0 N \lambda^2 i_1 / 4\pi^2 = \frac{3}{2\lambda} I_0 N (i_1/a^3)\frac{4}{3}\pi r^3 \quad (1)$$

$$I_2 = I_0 N \lambda^2 i_2 / 4\pi^2 = \frac{3}{2\lambda} I_0 N (i_2/a^3)\frac{4}{3}\pi r^3 \quad (2)$$

with $I_{1,2}$ = intensity per unit solid angle scattered when N particles are illuminated by one unit of intensity of polarized light of wavelength, λ

λ = wavelength of light in scattering medium.

r = radius of the (spherical) scattering particles.

I_0 = intensity of polarized incident beam.

N = number of illuminated particles.

$a = \frac{2\pi r}{\lambda}$

Thus, if the size and number of particles remains the same, the response per unit volume at one wavelength, $(i_1 - i_2)/a^3$, can be determined experimentally by varying the wavelength and multiplying λ times the measured quantity $(I_1 - I_2)$.

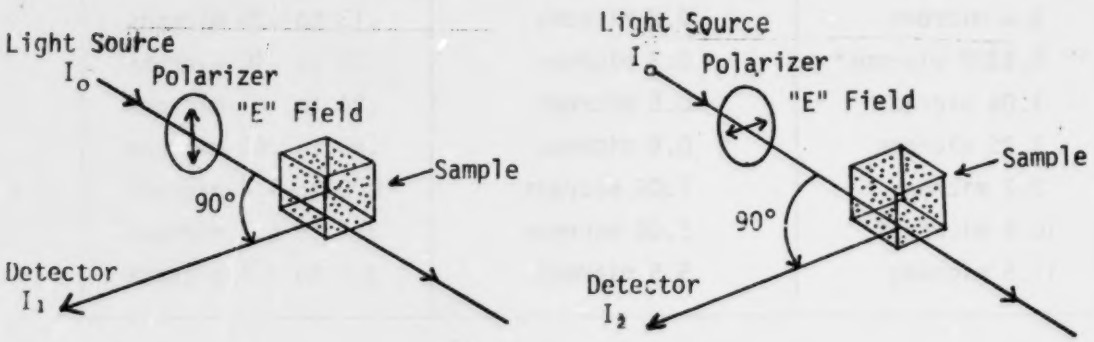

Figure 3. Configurations for 90° scattering for polarizations of light

The values for i_1 and i_2 are the scattering functions for the polarizations perpendicular and parallel to the plane of observation, respectively. These functions depend on a, θ, and n, where θ is the scattering angle and n is the ratio of the refractive index of the particle to that of the dispersant. Figure 4 shows a plot of $|i_1 - i_2|/a^3$ vs. a for n = 1.2 and θ = 90°. By changing λ, the diameter corresponding to the maximum around a = 1.6 changes. This procedure is used to scan the particle size distribution, thereby creating a histogram of the distribution.

Experiments were performed to verify these theoretical results. A spectrophotofluorometer shown in Figure 5 was used to measure 90° scattering of polystyrene spheres dispersed in deionized water at 10 ppm. The ratio of I_S to I_R (scatter and reference signals, respectively) was measured for two orthogonal polarizations and for sphere diameters of .234μ and .801μ. For each particle size, the monochromaters were scanned from .35μ to .65μ. The value $\lambda |I_1 - I_2|$ was plotted, normalized to peak at a = 1.6 for comparison to the theoretical plot of $|i_1 - i_2|/a^3$, (the dashed line curves in Figure 4).

Qualitative agreement between theory and experiment is evident. The dominant feature, the large response lobe at approximately a = 1.6, is quite evident. Similarly, the smaller alternating positive and negative lobes are observed for "a" between 4 and 7. The lack of quantitative agreement between these two plots is due primarily to the difference in reflectivity of the beam-splitter for the two polarizations. Also, exact angular adjustment of the polarizer was difficult in this instrument.

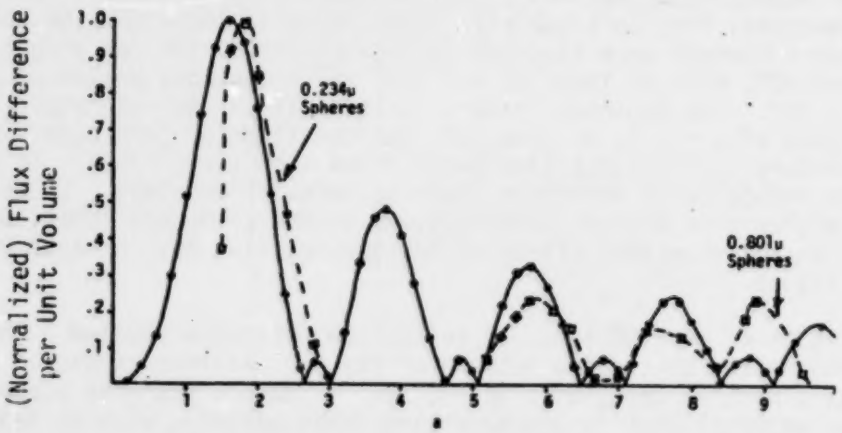

Figure 4. Experiment & theory for polystyrene spheres in water, n = 1.20.

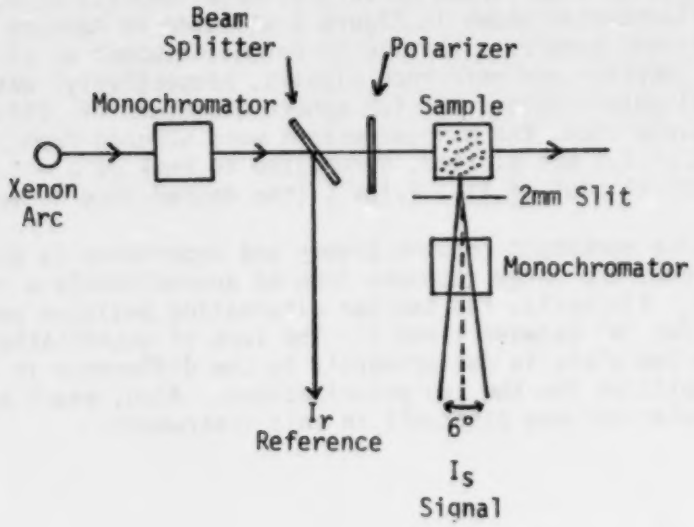

Figure 5. Spectrophotofluorometer System Used for Experimental Data in Figure 4.

ADDITIONAL THEORY & EXPERIMENTS ON 90° SCATTERING

After the start of the contract, a computer program was written, based on a subroutine obtained from IBM[5], to generate data on the volumetric response from rigorous computations of Mie scattering coefficients. One set of curves generated from this analysis (see Figure 6) shows how the volumetric response changes as a function of angular collection for acceptance angles around 90°, with an index of n = 1.5, and acceptance angles of $\pm$ 1°, $\pm$ 10°, and $\pm$ 20°. The dominant feature is the peak in the volumetric response in the vicinity of a = 1.5, as expected, but the items of particular interest are the secondary oscillations (indicated + and - on the curves). It is desirable to reduce these secondary lobes to zero, if possible. Larger acceptance angles give smaller contributions to the secondary lobes, owing principally to the smoothing effect of integrating flux over a range of scattering angles.

The effects of varying index of refraction were also studied. The effect of absorption on the scattering pattern of fly ash was investigated. This material has a nominal index of 1.96 - 0.66i. Figure 7 presents a curve for a fictitious material that is non-absorbing (transparent), with an index of 1.96 - 0.0i. The secondary lobe dominates this pattern. Figure 8 shows the response for an actual material, indicating the smoothing effects of absorption. This effect is related to well known phenomenon of how optical extinction coefficients are smoothed as a function of absorption.

An experimental system was then assembled, incorporating a lock-in amplifier and an electronic ratio circuit to measure 90° Mie scattering more accurately. This system enabled recording of continuous scattering curves for both polarizations, I_1 and I_2; hence, the response curve for the function $(I_1 - I_2)\lambda$ could be generated easily.

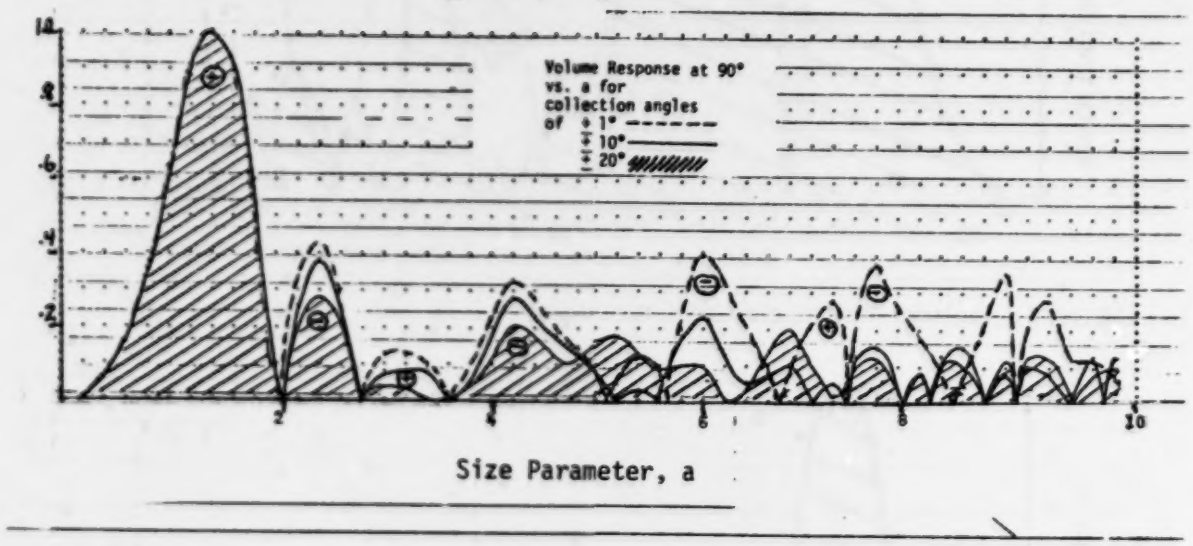

Figure 6: Volume response for different collection angles around 90°.

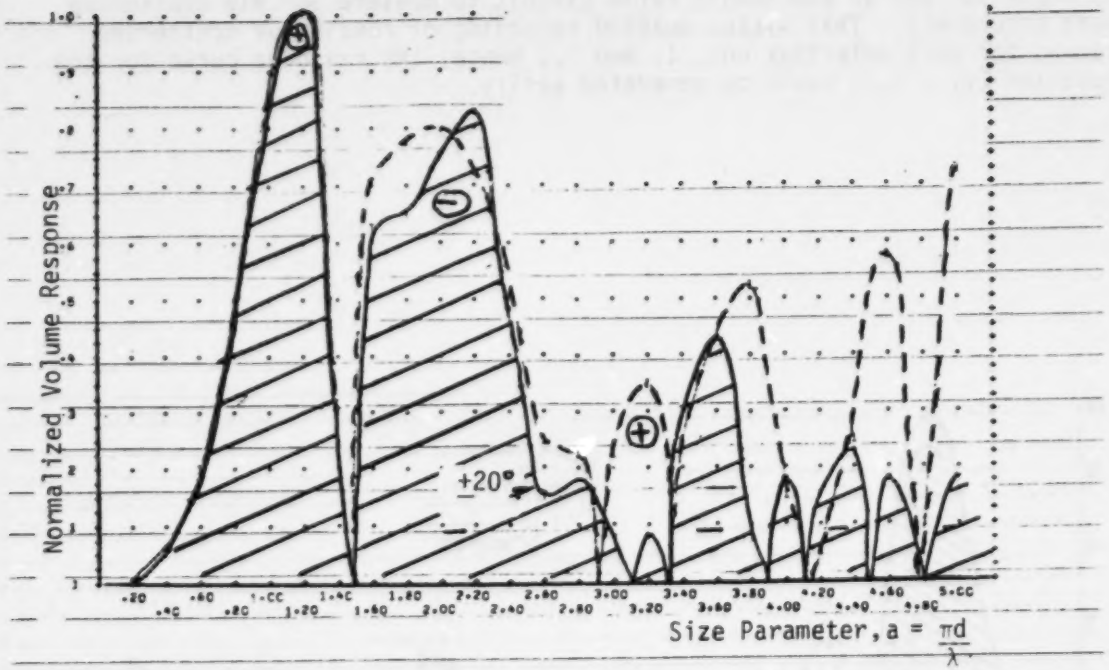

Figure 7. Volume Response at 90° for index = 1.96 - 0i

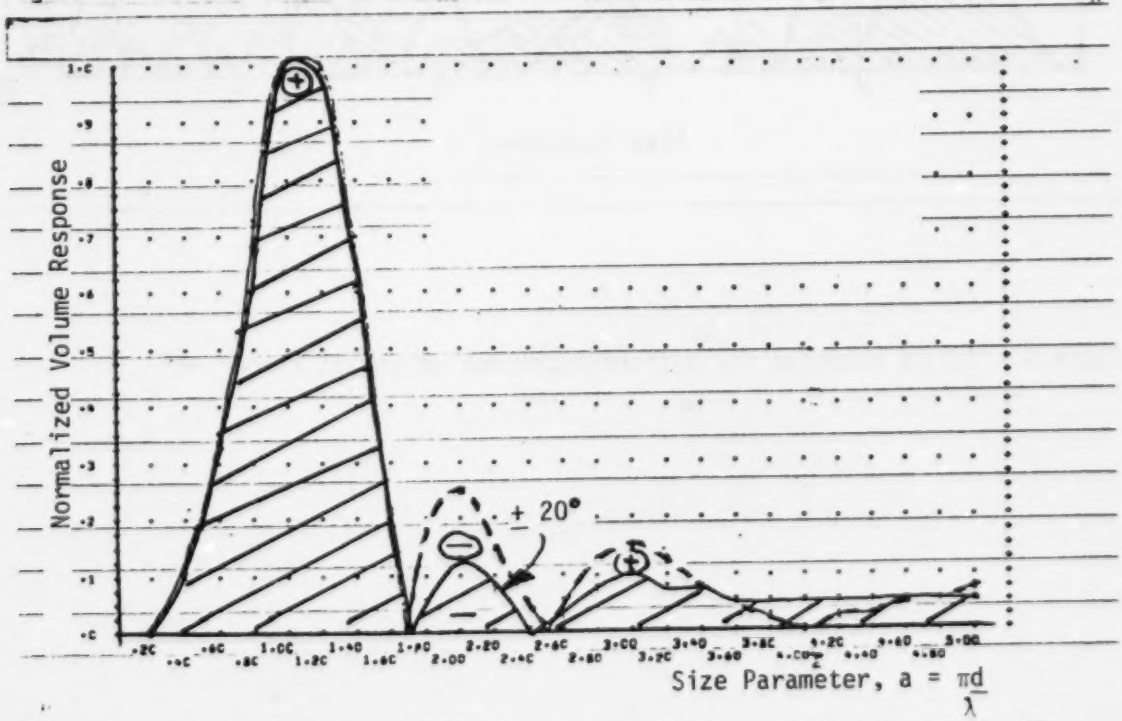

Figure 8. Volume Response at 90° for index = 1.96 - 0.66i (absorptive fly ash)

The experimental system, shown in Figure 9, consisted of a xenon arc, EG&G monochromator, and two U.D.T. PIN diodes. The source flux was chopped so that a P.A.R. 186-A lock-in amplifier could be used to filter ambient radiation noise from the relatively small 90° scattering signal. The flux passing directly through the sample was focused onto a PIN 6DP diode. This reference signal was electronically filtered to present a D.C. signal to an analog divider, which ratioed the scattered and reference signals to correct for spectral variations in source intensity. Therefore, the output of the divider was directly proportional to I_1 or I_2. While a rotating prism polarizer alternately selected I_1 or I_2, a synchronous motor scanned the monochromotor from 400 nm to 800 nm at a speed chosen so that a pair of measurements, I_1 and I_2, were recorded once every 5nm on a chart recorder.

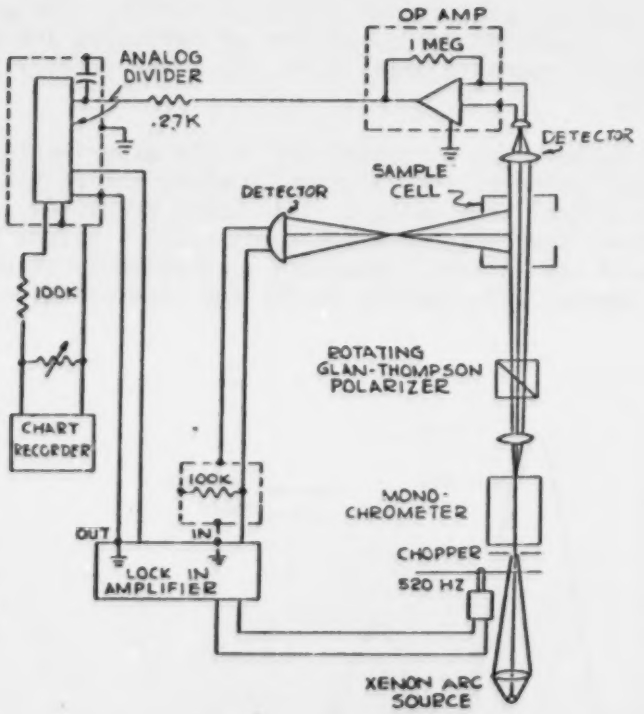

Figure 9. Schematic drawing of laboratory system used to verify the volumetric response functions for 90° scattering.

This system was used to record data for .312 micron and .801 micron polystyrene spheres, dispersed in a solution of 1% Triton X-100 in deionized water at 20 ppm. These two particle sizes generated scattering data for "a" values from 1.64 to 3.27 and 4.19 to 8.39, respectively. The angular scattering field was 20° centered at 90° with respect to the incident beam. The experimental results are plotted along with the theoretical response curve for comparison (see Figure 10). Notice that the experimental data agrees well with theory, both quantitatively and with respect to positions of extrema. The only major disagreement occurs in the region around "a" = 2.8, where the scattering signal became too low for accurate operation of the analog divider.

Further experiments were performed to confirm the selective reduction of secondary response peaks for absorbing materials. 90° scattering data was recorded for transparent and dyed (absorbing) polystyrene spheres of .234μ and .801μ diameter. This data is plotted along with a theoretical curve for non-absorbing particles in Figure 11. Notice the excellent agreement between experiment and theory for non-absorbing particles, and the selective reduction of the secondary response peaks for absorbing particles. The primary peak data (d = .234μ) for absorbing and non-absorbing particles are almost identical, but the secondary response peaks (d = .801μ) are greatly reduced for absorbing particles.

There are two factors not accounted for in the experimental data. Background molecular scattering of the solution in which the particles are suspended prevents the signal from going to zero where predicted. Also, the changes in refractive index with wavelength may cause a slight shifting of the location of peaks and valleys. However, even without correcting for these factors, the experimental data appears to fit the theoretical curve quite well.

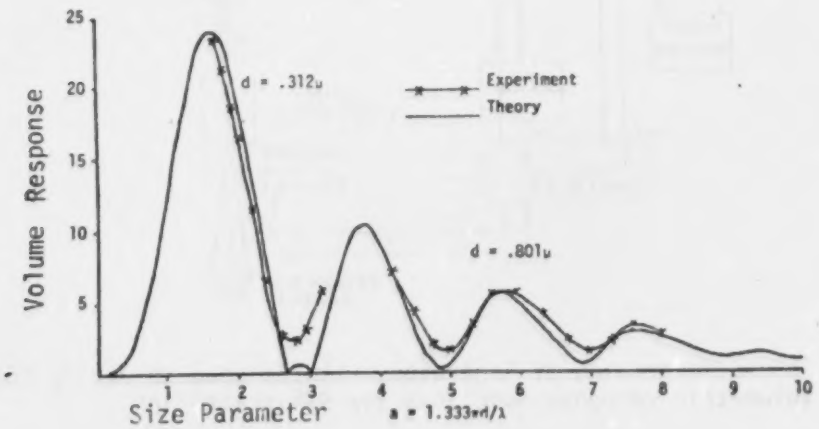

Figure 10. Experiments using system in Figure 9, with polystyrene spheres in water.

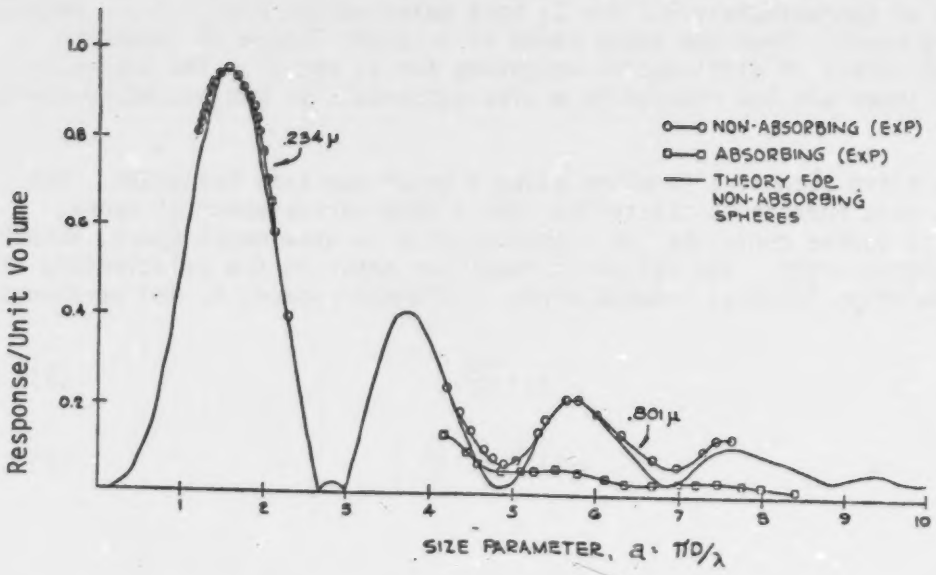

Figure 11. Theoretical and experimental curves for 90° scattering using absorbing and transparent material, showing the flux difference, $i_1 - i_2$, per unit volume of material. Two sizes of polystyrene spheres were used, 0.234 and 0.801 microns in diameter, and the wavelength was varied to change the size parameter, a.

REFINEMENTS OF THE 90° SCATTERING RESPONSE

Response functions for typical stack materials were evaluated during this phase and three methods were investigated for reduction of the secondary lobes in the scattering signals.

1. Widen the flux collection field angle.
2. Differentially weight the polarization components I_1 and I_2.
3. Broaden the spectral bandwidth of the source to convolve the response curve.

The effect of increasing flux collection field angle is illustrated in Figure 6. As the collection angle is increased to a 40° full field, with uniform weighting of contributions, the secondary lobes are reduced significantly.

The second method involves reducing the weighting factor of I_2 in the $I_1 - I_2$ response function. Theoretical studies show that most of the large secondary lobes are negative for refractive indices greater than 1.5. Since the primary response peak is positive, these secondary lobes can be selectively reduced without losing primary peak response. Studies indicated that a factor of approximately 0.7 for I_2 best balanced the positive and negative secondary peaks. Over the index range of interest Figure 12 shows the resultant effect of differential weighting for I_1 and I_2. The secondary negative lobes are now reduced to a size comparable to the secondary positive peaks.

The third technique involves using a broad spectral bandwidth. All previous data represents scattering over a very narrow spectral range. A broad band source convolves the response curve in wavelength space, smoothing the secondary lobes. The following equations describe the relationship of the convolution interval between alpha or diameter space, a, and wavelength space:

$$a = \frac{\pi d}{\lambda}, \tag{3}$$

so

$$|\Delta a| \simeq \left| a \frac{\Delta \lambda}{\lambda} \right| \tag{4}$$

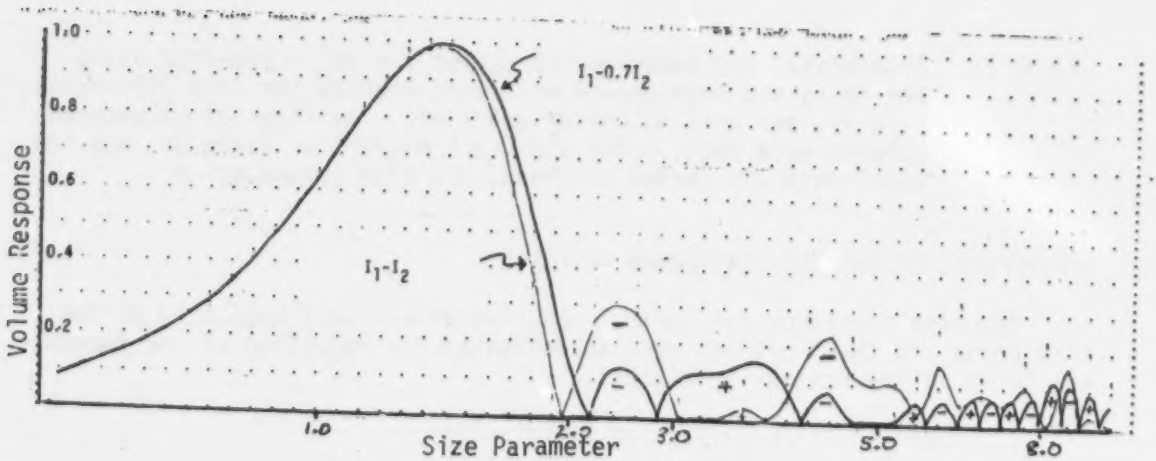

Figure 12. Comparison of different weightings of the difference, $I_1 - KI_2$

For constant $\frac{\Delta\lambda}{\lambda}$, Δa increases with a. Hence a broad spectral bandwidth causes each point fh the convolved response curve to represent a summation of points over larger alpha intervals as alpha increases. Thus, wavelength convolution has little effect on the primary peak, but a greater and greater smooting effect on secondary lobes.

The results of spectral convolution are shown in Figure 13. Note that the primary peak shows little change with increase in $\frac{\Delta\lambda}{\lambda}$ but the secondary peaks are reduced significantly due to the larger a convolution interval.

The combination of wide collection angle, differential weighting, and wide spectral bandwidth is generally effective in reducing secondary peaks to a negligible level for "a" greater than 5.

The 0.7 factor for I_2 causes a train of alternating plus and minus peaks of comparable size and the spectral convolution smears these peaks together; so they tend to cancel each other. The small secondary response which remains between alpha of 2 and 5 can be reduced through additional data processing.

Another study showed the variation in response as a function of the refractive index of the material. The peak of the response curve remains fairly stable as the index is changed, but the total scattered light energy for a range of particle sizes in the region of the response peak varies somewhat. Figure 14 presents the integral of the scattered energy as a function of the real and absorbing parts of the refractive index. Over the range of material studied, a factor of two in scattered light energy can result. This, however, is not of concern unless the material being measured has significant differences in composition as a function of size.

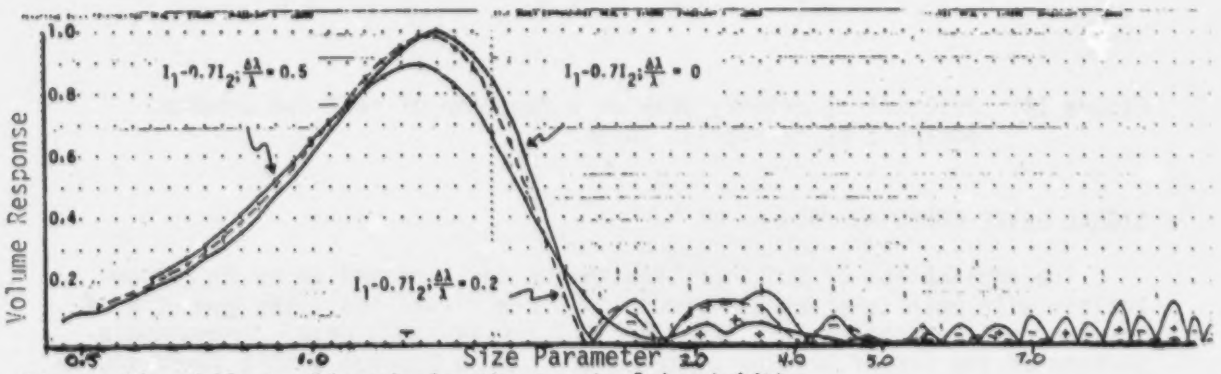

Figure 13: Effect of broadening the spectral bandwidth.

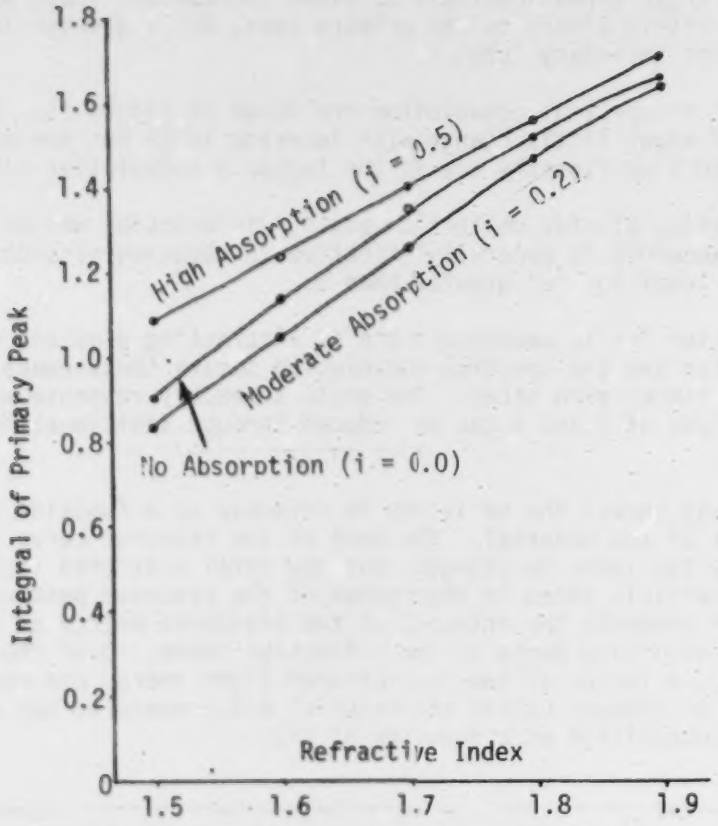

Figure 14. Integral of primary peak as a function of real and complex portions of refractive index.

SIGNAL LEVEL COMPUTATIONS

The application of 90° light scattering was proposed so as to be compatible with both in-stack and remote in-plume situations. The geometry of the two cases are shown in Figure 15. For the in-stack case, a reasonable section of the center portion of the stack can be covered with a fixed source and a detector of appropriate angular divergence. A thermal source or multiple lasers could be used. If necessary, both the source(s) and detector could be gimbaled to cover a range of locations within the stack such that the axes remain perpendicular. It is expected, however, that some reasonable assumptions about the distribution could allow a fixed source and detector, thus allowing a mechanically simple execution.

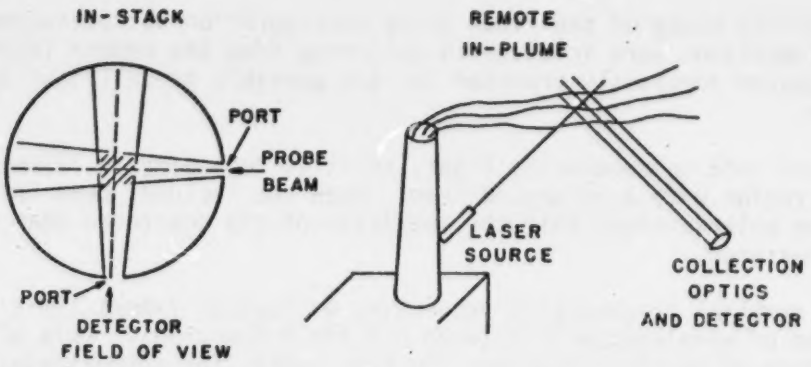

Figure 15. Stack and remote configurations for particulate size monitor, as originally proposed.

An in-plume measurement would require laser sources due to the limitations in intensity and directionality of conventional sources. However, the theory of operations remains unchanged. The detector and the laser need to be separated from each other and aligned so both are directed at the same point in the plume, while making an angle of intersection with respect to each other of 90°.

To evaluate the methodology, emphasis was placed on the in-stack configuration. A study was undertaken of the signal levels in a stack implementation for 90° scattering, when used to measure the size range of 0.2 to 10 microns. The study showed that the signal to noise ratio was less than one for thermal sources and conventional detectors at wavelengths greater than 2.3 microns. The use of lasers is indicated to provide sufficient power for measurements at 10.6 micron wavelength (5 micron diameter), and 77°K cooled detectors are necessary for measurements at 4.6 and 10.6 microns wavelength (2.3 and 5 microns diameter).

Due to the high cost of the optical sources and detectors necessary to extend the operation of the instrument far into the infrared, and the additional complexity of using a multiple source approach, a decision was made to consider modifications to remote sensing of 90 degree scattering.

STUDIES OF ALTERNATE CONFIGURATIONS

Through communications and meetings with the Project Officer, it was agreed to investigate modifications to the original proposal. An insertable probe configuration seemed to be the most attractive approach, combined with the use of fiber optic cables to collect the scattered light at the point of measurement and bring the optical signals outside the stack to be sensed with

conventional detectors.

ANALYSIS OF THE USE OF A FIBER PROBE FOR 90° SCATTERING

A feasibility study of the fiber probe configuration was performed. Several considerations were involved in switching from the remote (port-hole based) system previously proposed to the portable probe (fiber optics based) system.

1. Fibers tend to depolarize light, so it is necessary to illuminate the region with a polarized beam. When the incident beam has a known polarization, only the intensity of the scattered beam need be measured.

2. The spectral transmission properties of typical fibers limit the range of wavelengths to between 0.4 and 2.0 microns. This allows a range of particle response function peaks from approximately 0.2 to 1.0 microns.

3. The operating temperature in the stack can be as high as 260°C, but special fibers are available that can withstand this temperature.

4. Since the fiber is much closer to the scattering volume, flux is collected over a much larger range of angles than for the remote case. As shown earlier, this was found to help in smoothing the response curves.

This initial examination showed fibers to have advantages over remote sensing for submicron particles but raised a question about ability to measure the size fractions above 1 micron in diameter.

FORWARD SCATTERING CONFIGURATIONS FOR LARGE PARTICLES

As an alternative to using long wavelengths and exotic optics for measuring large particles, forward scattering was considered in combination with 90° scattering. Studies were performed on several configurations. One specific approach, evaluated in the early stages of system design, involved measuring scattering at both 90° and low forward angles, as shown in Figure 16. The light source is common for both modes. The forward scattering measurement is made by using a mirror or prism reflector at the end of the insertable probe to return a portion of the incident beam.

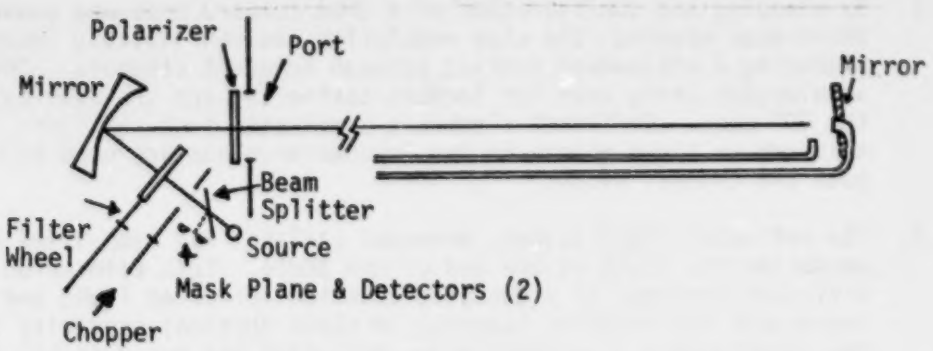

Figure 16. 90° scatter system with forward scattering capabilities.

During March of 1977 we met with the Technical Project Officer to discuss some of the configuration options, and it was agreed to combine the two modes in an insertable probe configuration using fiber optics.

Following that meeting, extensive analysis was performed on forward and 90° scattering combinations. Several changes and improvements were made, as listed below:

1. An arc source was selected instead of the tungsten lamp.

2. Only two channels were to be measured using the 90° scattering approach, at 0.421 microns and 0.850 microns in wavelength. These wavelengths were later changed to 0.45 and 0.9 microns.

3. Three channels were to be measured using a conventional forward scattering configuration, with the same wavelengths as for the 90° scattering.

4. The forward scattered light is measured at the end of the probe in the stack by use of three additional fiber bundles and a one inch diameter lens located at the end of the probe.

The advantages for each of the above features is listed below:

1. A tungsten source is sensitive to damage from vibrations and has a relatively large filament. The arc source is more stable in a vibrating environment. It has a more concentrated area of light, which is more readily focused or collimated. This provides a well defined beam, especially suited for the anticipated forward scattering work.

2. The third channel at 90°, which was to use light at about 1.7 microns, would have required an additional set of detectors, special polarizers, and very expensive fiber optic glass. It was found that a forward scattering channel could be substituted for the 90° channel

in the particle size region of 0.8 to 1.6 microns.

3. By changing the configuration of a true forward mode and adding a third mask opening, the size resolution was considerably improved, producing a minimum of overlap between adjacent channels. The wavelengths being used for forward scattering are the same as for the 90° case. Different algebraic combinations of the flux measured at three points in the Fraunhofer plane are used to compute the channel widths.

4. The reflected light system, proposed earlier, was simplified by measuring the light at the end of the probe. This eliminated difficult problems of vignetting unwanted reflected light and locating a mask and detector assembly in close physical proximity to the light source. Improved size resolution was not possible in the original configuration due to the limits on the range of angles which could be measured using a fixed reflector.

OPTICAL BACKGROUND MEASUREMENTS

A laboratory system was set up to make background and scatter signal measurements under conditions resembling the configuration of the planned prototype instrument.

A photomultiplier tube was used for the detector to measure the background since some signals were lower than the range of sensitivity of the silicon detector. For a given angle, the highest background levels were found to exist for the shortest wavelengths.

Optical background levels were measured for different angles and wavelengths in the forward configuration. The intensity of the main beam was measured with the same optical system by using neutral density filters to attenuate the beam. These filters were calibrated in a separate test. A ratio of background light to incident light was then computed, which removed any need to make absolute calibration of the individual components. The results are shown in Table 2.

Table 2: Background Normalized to Input Beam*

Angle	λ = .4500	λ = .6500
3.8°	1.1×10^{-8}	---
4.8°	7.3×10^{-9}	2.0×10^{-9}
7.5°	3.9×10^{-9}	1.0×10^{-9}
10.3°	2.7×10^{-9}	6.8×10^{-10}
90° ($\pm$1°)	6.5×10^{-11}	---

* Expressed as a fraction of the main beam

Note the significantly lower background measurements at the longer wavelength and the very low value at 90°.

Several experiments were attempted to define the source(s) of the background signals in the forward direction. The most dramatic improvement was achieved by purging the sample region with dry nitrogen. In the forward scattering mode, the background signal dropped significantly at all measured forward angles when the ambient room air in a transparent tube was replaced by flowing dry nitrogen. The resultant data appears in Table 3, and implies that approximately 90% of the background light level observed in the forward direction is due to light scattered from components (dust, moisture, etc.) in ambient room air. The remaining background contributions are probably due to molecular scattering and residual diffraction effects from the beam forming optics.

Table 3: Sample Region Purged with Dry Nitrogen

Angle	Background with Dry Nitrogen (Referenced to Main Beam)	Reduction (%) over Ambient Air 76° and 70% Rel. Humidity
4.75°	3.06×10^{-9}	-58%
7.50°	4.08×10^{-10}	-90%
10.25°	4.49×10^{-10}	-83%

During the course of these experiments, some variations in the background levels were observed in ambient air, perhaps related to changes in humidity in the laboratory due to prevailing weather conditions. Figure 17 provides a graph of the background level as a function of angle, as measured for three different situations, two in ambient air, and one in dry nitrogen.

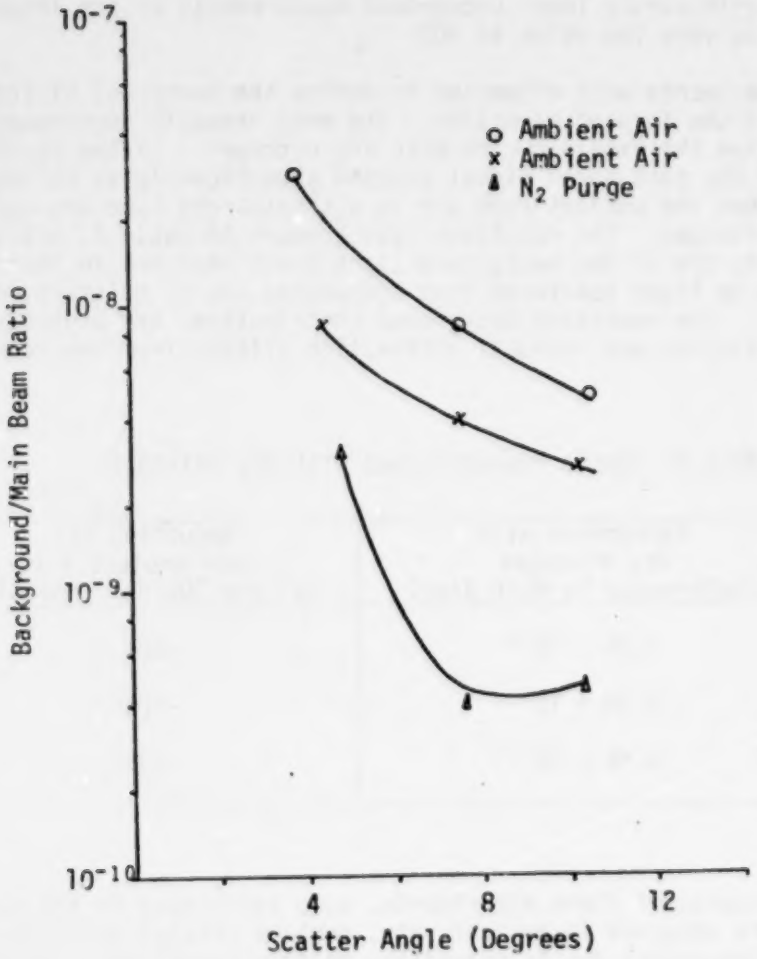

Figure 17. Background/Main Beam Ratio vs. Scatter Angle

Other experiments were performed to determine the background effects of scattering from dirty windows and refraction due to thermal gradients. Background readings were taken at $\Theta = 4.75^{o}$, 7.5^{o}, and 10.5^{o} for three cases:

1. With dirty glass window on the probe side of the beam forming lens.
2. With dirty glass window directly in front of collector lens.
3. Hot air flowing through the sample region of the probe.

In all three cases, no significant change in background was observed.

SECTION 4

THEORY OF INSTRUMENT DESIGN

This section describes the design of the instrument: its operating environment, optical design, component selection, electronic filter for noise suppression, purge system, and air curtain design for protecting optical surfaces in the stack from contamination, and then, a brief overall description of the instrument.

OPERATING ENVIRONMENT

Application to oil and coal combustion processes at various field locations requires an instrument to meet diverse operating, measurement, and deployment conditions. In addition, an on-stack instrument must withstand the rigors of vibration, corrosion and gas flow variabilities, characteristic of in-situ measurements. Within a duct, the probe may be exposed to temperatures between 90° and 260°C, gas velocities up to 18 meters/second, and acid and water vapors and condensation as well as the fouling effects of particulate. Particles of interest range between 0.1 and 10 microns in diameter, have a specific gravity near 2.5 and indices of refraction in the range of 1.5. The size distribution may be broad, evenly spanning the instrument five size channels; or narrow, with as much as 80% in a single measurement channel. Total loadings are anticipated to fall between 0.01 and 0.1 grams per cubic meter (4-40 ppb) while the instrument's measurement span extends to 1.0 grams per cubic meter. At controlled intervals, precipitator rapping creates more dense, transitory clouds of particulate.

The instrument is to be used at a variety of sites where access to the sampling point may be restricted to a four inch port and service limited to 110 volt power. Near the sampling point, instrumentation will be exposed to combustion fumes, particulate, and the weather and protected only be a tarpaulin.

OPTICAL DESIGN

The interior stack temperatures rule out the use of in-situ detectors, so a set of high temperature fiber optic cables are utilized to sense the scattered light at five points(three forward angles and two orthogonal positions at 90° to the probe beam). These cables are installed inside a 1.5 meter long stainless steel tube, whose outside dimension is approximately 9

cm. The active sensing region is towards the tip of the probe and is a slot 36 cm long by 3 cm wide. A lens located in the tube tip collects scattered flux for the forward angles, while the two 90° fibers look directly through protective windows and air curtains into the sample region. Each fiber cable runs to an individual detector, located in the transceiver outside the stack, at the end of the probe. A sixth detector is used to monitor beam strength, as reflected from a tilted glass plate in the transceiver section.

The chopped optical probe beam is generated by a xenon arc source and chopper wheel, located in the transceiver. Thin-film interference filters with center wavelengths of 0.45 and 0.90 microns are combined with linear polarizers in an indexing filter wheel. The filtered light falls onto a pinhole, which serves to adjust beam position, and then passes down the center of the tube in a nearly collimated beam of alternating blue or infrared polarized light, with a beam diameter of approximately 1.25 cm. To avoid spurious signals the light beam is not reflected internally, but exits the probe through a hole at the tip. A schematic drawing of the optical system is shown in Figure 18.

SPECTRAL BALANCE

The components in the optical system were selected so that equal loadings of particles in either the blue or the infrared beams generate nearly equal detector outputs and full scale readings at the computer input. In general, less flux is scattered from the infrared beam than is scattered from the blue beam, but better transmission through the fiber optic bundles and response to infrared by the silicon detectors actually produce higher detector outputs for the infrared beam. To equalize outputs, a neutral density filter (with 70% transmission) was inserted into the infrared beam.

Other techniques for improving the sensitivity and spectral balance of the optical system were investigated and discarded. Substitution of a mercury bulb for a xenon doubled the power of the blue beam but decreased the infrared power by a factor of five, resulting in an overall loss in instrument sensitivity. Specifications of photomultiplier tubes indicated a potential 10 fold improvement in detection of scattered blue light but only comparable performance in the infrared region. The increased technical requirements and expense of these detectors outweighed this performance advantage. Silicon avalanche detectors were rejected because commercial units required more electronic support and could only match the performance of the common, large area silicon detectors used in the final design.

The fiber optic bundles have stainless steel jackets and incorporate commercial fibers with specially molded ends secured with Emerson & Cummings 2762 FT high temperature epoxy (good to 315 C°). Of possible vendors, only Dolan-Jenner, Inc. had stock molds for producing tight bends and custom dimensions needed in the probe.

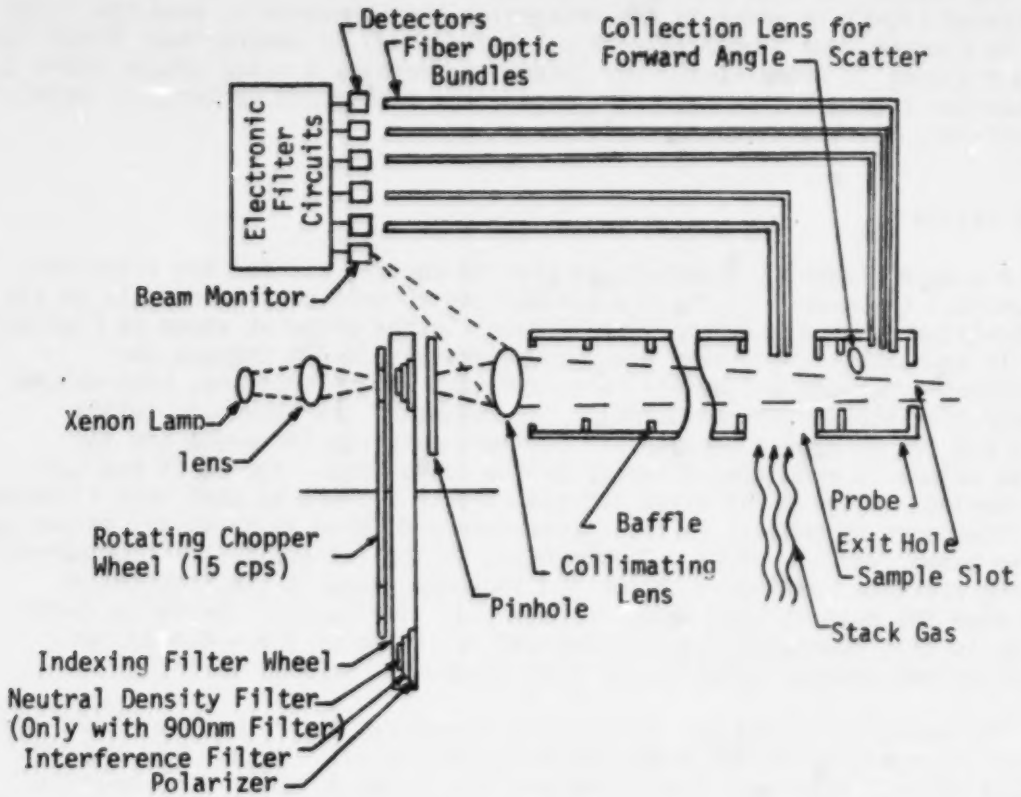

Figure 18. Schematic Drawing of Optical System

ELECTRONIC FILTER

The power of the light scattered by particles, collected by the fiber optics and relayed to the silicon detectors is as little as 10^{-12} watts. Model HUV-4000B silicon detectors, made by EG&G, were selected because these detector-amplifier assemblies offered signal gains in the order of 10^{8} and low level noise by virtue of component selection and hybrid construction. To improve noise rejection each amplifier is followed by a switched filter circuit which responds to the frequency of the chopped probe beam (15 cps) but rejects higher and lower frequency signals and has an effective bandwidth in the order of 10 cps.

The circuit is shown in Figure 19 and, operationally, consists of a switched up/down integrator to achieve a low-noise response. Light chopped at 15 Hz impinges on the photodiode detector and the diode amplifier charges

and discharges the coupling capacitor (100μf) without saturating. (The capacitor negates the amplifier drift and off-set.) The integrator's input I_I is sequenced by switches S_1 and S_2 between outputs O_A and $-O_A$ to achieve up/down integration of the scatter signal. These switches are synchronized with the chopper so that when the light beam is projected, the signal (scattered light) is added in the integrator and, conversely, when the light beam is blanked, the signal (electrical background) is subtracted. Since the chopper timing is symmetrical, the integrator retains a value proportional to the scatter signal and cancels out longer term background variations, detector off-set, and low frequency noise.

PURGE SYSTEM

A single blower is used both to provide cooling air for the electronic and optical components in the transceiver and to deliver filtered air to the air curtains which protect optical surfaces in the probe as shown in Figure 20. In operation, the blower draws approximately 20 CFM through the transceiver, through a flexible hose, and into a high pressure, high volume regenerative blower (Rotron SL4P2). The output of the blower is split; about 2-8 CFM is driven through air delivery hoses to the probe and the excess volume is exhausted directly to the atmosphere. The inlet and outlet openings in the transceiver are sealed with filters so that only filtered air flows over components in the transceiver and twice filtered air passes on to the blower and the probe. The mounting of the filters to the transceiver's housing provides continuous protection for components in the transceiver even when the hose to the blower is detached. The Balston (Grade D) filter tubes, in this configuration, provide 99% retention of 0.3 - 0.5 micron particles and greater retention of both larger and smaller particles.

The velocity of the gas in the duct determines the flow rate of the air to the air curtains in the probe which is controlled by an orifice and the exhaust valve. When duct velocities are low, a small restricting orifice is employed to limit the flow to the probe and yet permit high volume flow through the transceiver and blower for cooling purposes. (High flow through the blower prevents thermal cut out of the Rotron motor.) When higher duct velocities prevail, less restrictive orifices are used to provide greater flow to the probe. Finer adjustments are made with a manual exhaust valve.

After the orifice at the blower, the flow to the probe is divided and delivered through five 1½ cm diameter hoses and then, inside the probe, through 1¼ cm stainless steel tubes to the air curtains. Balancing of the flow to each air curtain is accomplished by throttling orifices located in the delivery connections to the probe. The large delivery hose and tube diameters produce moderate pressure drops, in the vicinity of 10-40 inches, which serve to moderate the effects of pressure fluctuations in the stack.

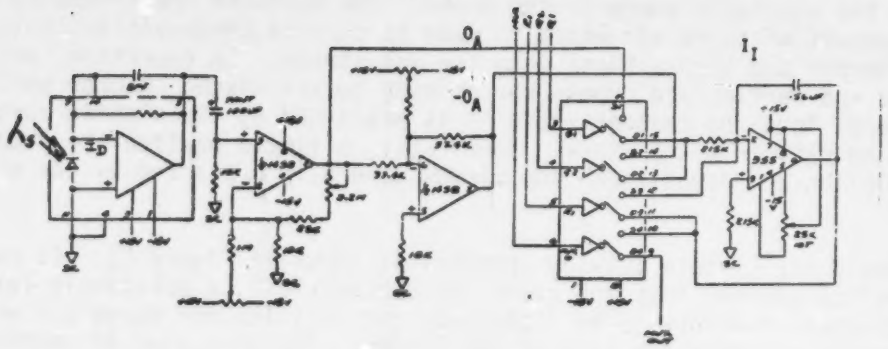

Figure 19: Schematic Drawing of Electronic Filter Circuit

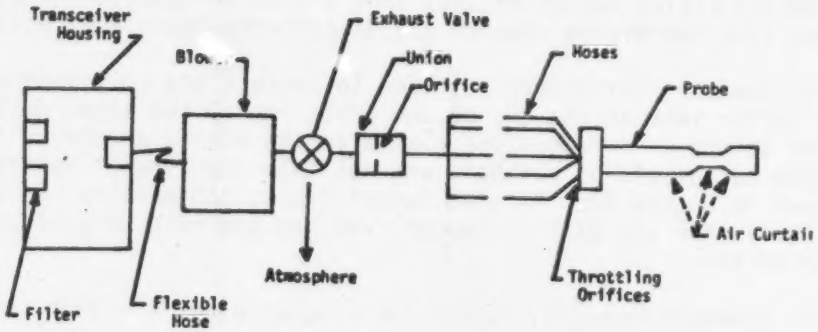

Figure 20: Schematic Drawing of Blower and Pneumatic Components

AIR CURTAINS

The optical surfaces which look into the sampling slot in the probe are sealed behind glass plates which are protected from fouling particulate by air curtains. The air curtains extend the time between cleanings to approximately 20-40 hours depending on stack conditions. The curtains are unusual in that they pass widely diverging light rays, are located in close proximity to the sampling area without blowing away sample, and are small enough to fit into the available space in the probe. The curtains are formed by only a small amount of purge air which is made to circulate non-violently in a mixing chamber and then exhaust into the gas stream. In operation, most stack gas and particulate bypass the opening to the mixing chamber while a little seeps into the chamber where it is entrained by circulating purge air and carried back into the stack. Inevitably, a little particulate remains in circulation and deposits on the window generally protected by the mixing chamber.

A basic air curtain (mixing chamber) is shown in Figure 21. It consists of an orifice opening into the stack (or sample slot), a relatively large mixing chamber, a window to be protected, and an inlet for purge air which directs clean air over the face of the window. The direction of incoming purge air cooperates with the flow of the stack gas (beyond the orifice) to encourage circular flow in the mixing chamber. The volume of purge air is adjusted to generate a mixing line between the stack gas and purge air of 10 degrees as indicated by Ø. Higher purge flow rates (and greater mixing angles Ø) blows sample further away from the opening but does not appreciably improve performance. Reduction in flow rates to half this volume (and a mixing angle of 5^{o}) results in only modest loss in performance. Still lower rates, producing mixing angles of less than 5^{o}, allow substantial migration of stack gas into the mixing chamber and significant loss in effectiveness.

The air chambers (air curtains) used to protect the collimating lens and the collector lens at the tip of the probe employ the above design with the addition of one or more orifice plates in the mixing chamber. These plates create serial mixing chambers and multiple improvement in effectiveness as shown in Figure 22. In wind tunnel tests, the addition of an intermediate plate in the tip mixing chamber reduced the rate of contamination by a factor of ten.

The air chambers used to protect the windows over the fiber optic bundles at 90 degrees to the slot operate on the same principle but were drastically modified to meet severe space limitations. In these instances, the shallow depth dimension permitted only a shallow mixing volume that would not maintain consistent circular flow. The required flow is mechanically established by inserting a baffle which confines the incoming purge flow to a narrow dimension and imposes a tight, 180 degree bend on this stream as shown in Figure 23. A short overhanging lip completes the small chamber. In trials, the air curtain proved more effective with the lip than without one.

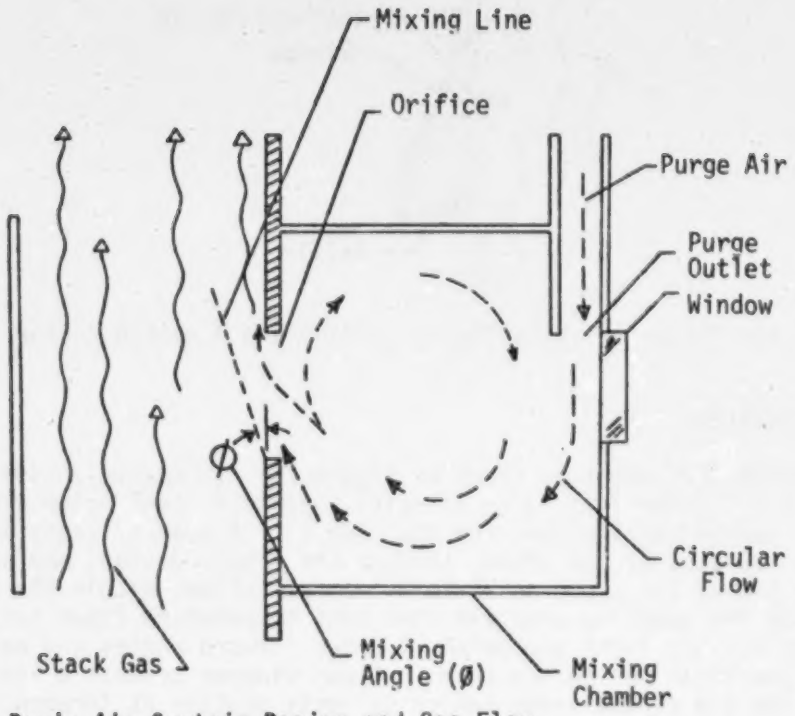

Figure 21. Basic Air Curtain Design and Gas Flow

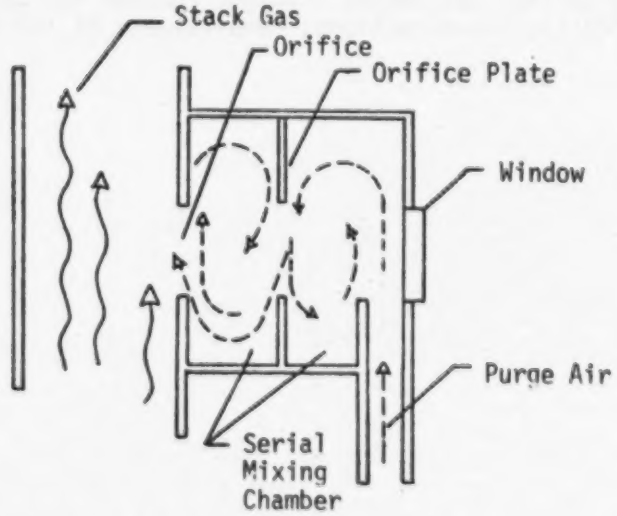

Figure 22. Air Chamber and an Additional Orifice Plate Used to Create Serial Mixing Chambers

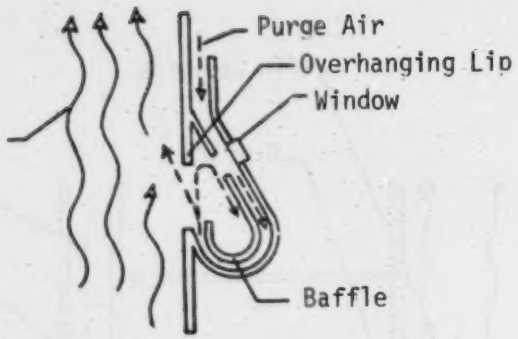

Figure 23. Air Chamber with Baffle to Confine and Direct Air Flow

SUMMARY DESCRIPTION

The entire instrument is shown in Figure 24. To sample inside a duct, it employs a 1.5 meter long, 9 cm diameter stainless steel probe with a 36 x 3 cm sample passage near its tip (Key 1). A beam of light is projected down the axis of the probe, through the sampling slot, and out through the tip of the probe so as to avoid reflections within the slot. Located about the sampling area are five high temperature fiber optic cables which collect light scattered at three forward angles and at two orthogonal positions 90° to the beam. Glass windows protect a lens located in the tip of the probe (which collects scatter at forward angles) and the faces of two 90° fibers which look directly into the slot. These windows are protected by air curtains which are formed by aerodynamic cavities and metered flows of filtered, purge air. Within the duct, the probe is oriented so that gas passes straight through the slot and its direction satisfies the one-directional requirements of the air curtains.

In the transceiver (Key 2), a xenon arc source and a rotating disc generate a beam chopped at 15 Hz. The beam passes through interference filters (with center wavelengths of .45 and .90 microns) and linear polarizers mounted on a filter wheel, through a pinhole, a collimating lens, and a protecting window and air curtain. A geneva mechanism indexes the filter wheel at one second intervals causing the polarized beam to alternate from blue to infrared light while the pinhole (and micrometer adjusting screws) centers the beam in the exit tube at the tip of the probe.

Light scattered in the sampling slot is returned by five fiber optic cables to silicon detectors located in the transceiver. A sixth detector collects reflected light from the beam. Filter circuitry associated with the detectors is synchronized with the chopping rate of the beam so as to negate extraneous noise and ambient light. The transceiver is enclosed by a light tight cover with four filter protected ports which pass cooling air.

The control console (Key 3) includes a microprocessor which reads twelve detector signals from the transceiver (five angular scattering signals and one beam strength signal for each of two colors). The signals are combined into five volumetric responses which are then decoupled using a matrix routine to produce a five channel histrogram of loadings on the printer (Key 4). Total loading and mean particle diameters are also reported on an LED display. Since computations normalize signals to beam strength, results are insensitive to minor contamination of the beam generating optics in the transceiver. Operator controls include a function switch for measuring and storing background signal values or making measurements in the stack. Five span ranges between 0-40 ppm and 0-400 ppm and eight sample periods between 2 and 256 seconds are available. To accomodate precipitator rapping within a sample period, individual one second samples which exceed the measurement range are excluded from computations but are reported as bad samples at the printer. Power to all subassemblies except the lamp is controlled at the console panel.

The air blower (Key 5) is used both to draw cooling air through the transceiver and to deliver purge air to the air curtains in the Probe. The xenon lamp (in the transceiver) is driven by a lamp power supply (Key 6) which is a standard unit (Model CA-75-8267, Illumination Industries, Inc.) packaged in a commercial drip proof enclosure.

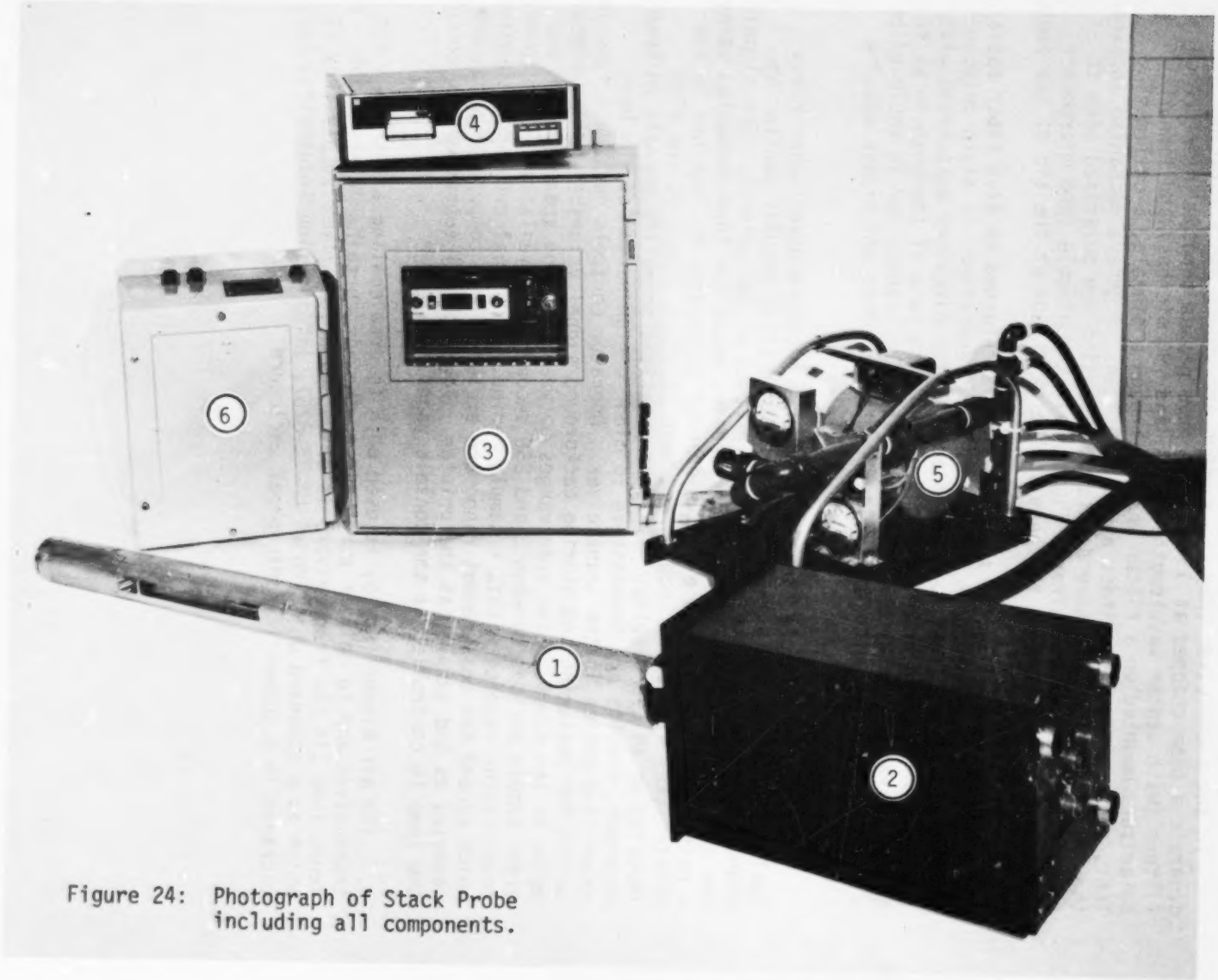

Figure 24: Photograph of Stack Probe including all components.

SECTION 5

TESTING OF THE PROTOTYPE

This portion of the report describes several phases of calibration and testing of the completed prototype. The first section discusses the theoretical calibration of the instrument as built. The next section describes controlled in-house testing of the unit to verify its performance. Sections three and four describe tests performed at Research Triangle Park at the EPA controlled source laboratory, and tests carried out at an East Coast coal-fired facility. During the testing phases several changes and modifications took place, and the most significant of these are described in the last section.

THEORETICAL CALIBRATION

This section summarizes the calculation procedure used in the final calibration of the EPA prototype stack monitor. In the process of calibration several assumptions were made, as listed below:

1. The particles are spherical[6], and rigorous scattering theory (Mie theory) is used to predict scattered light distributions.

2. The refractive index is that of silica, $n = 1.5 - 0.0i$, a common stack material.

3. The particle distribution is to be represented on a log diameter scale, within the range of 0.1 to 10 microns.

4. Five equal log increment intervals are to be measured, and within each interval, the distribution is approximately flat.

5. The density of the material is 2.5 grams/cm^3, which makes the loading of 0.01 to 0.1 grams/m^3 equivalent to 4 to 40 parts per billion by volume.

6. The electronic gains will be set to anticipate 40 parts/billion in any one of the five channels.

Two computer programs incorporating Mie scattering subroutines (supplied by IBM[5] and modified at L&N) were used for this analysis.

MIESCAT: This is a forward angle program which computes the flux in watts which passes through an aperture in the Fraunhofer plane of a forward

scattering optical system when a particle is illuminated by one watt per cm^2 of unpolarized light. Cosine fourth losses are included. Refractive index is an input parameter.

MIE: This program generates the Mie Coefficients i_1 and i_2, which are functions, the refractive index, n, the angle, Θ, and the size parameter, a, which is

$$a = \pi d/\lambda \tag{5}$$

Summation over angles is possible with individual loss coefficients, provided the coefficients and angles are symmetric about 90°. When one particle is illuminated by 1 watt per cm of polarized light, the scattered intensity per particle, per unit solid angle is

$$\frac{\lambda^2 i_1}{4\pi^2} \text{ or } \frac{\lambda^2 i_2}{4\pi^2} \tag{6}$$

with λ in cm.

Calculations were performed to predict signal levels to each of the five detectors in terms of radiant power for a given loading. The particle size distribution used for this analysis is flat on a logarithmic scale, with 1 part per billion by volume in each of the five channels. The sample regions are listed in Table 4 by particle diameter. The actual diameter values are taken from computer generated diameter intervals, with adjacent diameters having a ratio of 1.1297.

Table 4: Histogram Intervals for Prototype Instrument

Designation	Size Range (Diameter in Microns)	Log Interval	Measurement Wavelength (Microns)
A: "0.2"	0.114 to 0.268	.423	0.45
B: "0.4"	0.302 to 0.710	.423	0.90
C: "1.0"	0.802 to 1.884	.423	0.90
D: "3.0"	2.128 to 4.998	.423	0.45
E: "7.0"	5.646 to 13.259	.423	0.90

The three forward scattering channels range from 3 to 11 degrees. Descriptions of the collection apertures, as built, are listed in Table 5.

Table 5: Forward Channels

Angle	Instrument Designation	Radial Dimensions (Inches)	Width (Inches)	Area (cm^2)
3.9°	F5/45/95	.0477 to .0667	.044	.00539 cm^2
7.8°	F4/44/94	.0943 to .134	.103	.02638 cm^2
11°	F3/43/93	.134 to .196	.103	.04120 cm^2

Each of the zones was modeled using the MIESCAT program. Since the aperture definition for the program is based on a radial coordinate system and these apertures are rectangles, a slight adjustment of inner and outer radius was made, preserving the total area of the aperture.

Computer runs for an index of n = 1.5 - 0.0i were generated, and within each size range the average was calculated by summing the individual flux per unit volume of material values and dividing the number of log intervals.

Table 6 provides a list of parameters used in computing the power incident on each detector.

Table 6: Symbol Definitions

Symbol	Description	Units
W	Radiant Power Striking the Detector Face	Watts
L	The loading in parts/billion per log interval channel	Volume/Volume
V	The volume of material both illuminated and seen by the detector (including vignetting losses)	cm^3
d	Particle Diameter	Microns
I_0	The intensity of the source, as unpolarized light	Watts
T	The transmission of each window/lens/fiber train	———
F/d^3	The average power coefficient/d^3 per unit log interval, as computed from the MIESCAT program	$1/micron^3$
v	The volume of one spherical particle	$Micron^3$

The number of particles observed is expressed as

$$n_0 = L \frac{V}{v} \left| \frac{10^4 \text{ microns}}{\text{cm}} \right|^3 \qquad (7)$$

The calculation of W is done for each angle, Θ, size interval, S, and wavelength, λ. The resulting formula is

$$W(\Theta,S,\lambda) = L\ V(\Theta) \left[F(\Theta,S,\lambda)/d^3 \right] \frac{6}{\pi} \left[\frac{10^4 \text{ microns}}{\text{cm}} \right]^3 I_0(\lambda)\ T(\lambda,\Theta) \qquad (8)$$

The most difficult part of this procedure is the determination of common volume, V, including the effects of vignetting. Computation of the common volume is quite complicated with a non-point detector due to the off axis geometry of the lens system. An experimental approach was attempted, based on comparing the signal scattered for the actual aperture to the signal measured at a region of no vignetting for a 220 micron pinhole aperture.

Table 7 provides a summary of the experimental and theoretical results and also includes the experimentally determined transmission functions of lens/window/fiber combination. These transmission losses did not contribute to the experimental uncertainty in common volumes, since the calculations used ratios of signals at each wavelength.

Table 7: Volume and Transmission Factors

Channel	Common Volume (Experiment)	Common Volume (Calculations)	Transmission	
			Blue (0.45)	Red (0.90)
3 (11°)	5.5 $\pm$ 1.5	7.1 cm^3	.201	.334
4 (7.8°)	8.2 $\pm$ 2.0	10.1 cm^3	.232	.372
5 (3.9°)	17 $\pm$ 4.0	12.3 cm^3	.205	.352

Finally, the power of the probe beam was measured as .485 milliwatts in blue and .412 milliwatts in red. This was polarized light, so the equivalent intensity was 1/2 the measured intensity. When distributed over the 1/2 inch diameter beam, the intensity, I_0, was

$$I_0 = \begin{matrix} 1.914 \times 10^{-4} \text{ watts/cm}^2 \text{ (0.45 microns)} \\ 1.626 \times 10^{-4} \text{ watts/cm}^2 \text{ (0.90 microns)} \end{matrix} \qquad (9)$$

Using these coefficients, the power levels, W, were computed as listed in Table 8.

Table 8: Watts of Radiant Power for 1 Part/Billion per Channel

Wavelength	Size	3.9°	7.8°	11°
0.45μ ($.485 \times 10^{-3}$ watts)	A	5.7968 E-12	2.496 E-11	2.181 E-11
	B	5.8733 E-11	2.407 E-10	1.975 E-10
	C	5.576 E-11	1.631 E-10	8.863 E-11
	D	5.934 E-11	4.307 E-11	1.374 E-11
	E	5.596 E-12	8.771 E-12	2.952 E-12
0.90μ ($.412 \times 10^{-3}$ watts)	A	4.292 E-13	1.678 E-12	1.5245 E-12
	B	1.0471 E-11	4.185 E-11	3.804 E-11
	C	4.948 E-11	1.820 E-10	1.471 E-10
	D	4.602 E-11	9.700 E-11	4.189 E-11
	E	3.029 E-11	1.017 E-11	6.658 E-12

For the polarization measurements, two fiber bundles are oriented at 90° to the incident beam. The optical axes of these two fibers are perpendicular to each other, so the fibers see the two orthogonally polarized planes of scattered light.

The fiber faces are 0.5 inches (along the direction of the probe beam) by 0.024 inches, for a surface area of $7.742 \times 10^{-2} cm^2$. No lens or optical system is used, so the fibers collect over a wide angle, from 50° to 130°, with most of the sensitivity between 60° and 120°.

Using the expressions in (6) for scattered flux per unit solid angle, W, the power incident on each detector can be computed from,

$$W(p,S,\lambda) = \frac{LVT}{v} A/R^2 \; I_o \frac{\lambda^2}{4\pi^2} \; [i_p] \qquad (10)$$

Table 9 provides a list of parameters used in this equation.

Table 9: Terms Used in 90° Calculations

Symbol	Description	Units
W	Radiant power striking detector face, as function of size, S, polarization, p, and wavelength, λ	Watts
L	Loading, in parts per billion per log interval channel	---
V	Volume of region seen by fiber	cm^3
v	Volume of one spherical particle of diameter, d	cm^3
α	(Alpha) - dimensionless size parameter, $\pi d/\lambda$	---
T	Transmission of fiber bundle	---
I_p	Intensity of polarized light	$Watts/cm^2$
i_p	i_1 or i_2, as defined in equation 2	1/Steradians
A/R^2	Solid angle subtended by fiber face, with A, the area of the face and R the distance to a scattering object	Steradians

Due to the wide field of coverage, V, R, T, and i_p are all functions of the collection angle. Using the computer program, MIE, a numerical integration was performed over the range of 50° to 130°, for both polarizations, and the response per unit volume was summed over the appropriate log interval ranges.

The individual R_i and V_i values were computed from a scale drawing of the collection system. Experimental data on the fiber transmission was measured as a function of wavelength and angle. The MIE program then was used to calculate

$$M_p(\alpha) = 10 \sum_{\alpha} \sum_{\Theta} \frac{i_p(\theta)\ V(\theta)\ T(\theta)}{\alpha^3 R(\theta)^2} \qquad (11)$$

From this, equation (10) could be evaluated readily, as,

$$W = I_p \frac{3}{2} L A \frac{1}{\lambda} \frac{10^4 \text{ microns}}{\text{cm}} \frac{1}{8} \frac{1}{10} M_p(\alpha) \qquad (12)$$

based on the relationship

$$\frac{1}{V} = \frac{1}{\alpha^3} \frac{6\pi^2}{\lambda^3} \qquad (13)$$

The 1/8 factor in equation (12) is due to the summation in M over 8 intervals. The results are given in Table 10, expressed as watts of energy for 1 part per billion in each size range.

Table 10: 90° Signals for 1 Part/Billion

Size	i_1 90°		i_2 90°	
A (.2)	1.4912	E-11	4.0539	E-12
B (.4)	9.4152	E-12	1.1577	E-11
C (1.0)	3.4194	E-12	3.8246	E-12
D (3.0)	8.8710	E-13	8.0443	E-13
E (7.0)	2.0620	E-13	2.5974	E-13
A (.2)	1.8457	E-12	1.8271	E-13
B (.4)	7.9515	E-12	3.5484	E-12
C (1.0)	3.0741	E-12	4.2514	E-12
D (3.0)	7.8898	E-13	1.3776	E-12
E (7.0)	2.5030	E-13	2.6722	E-13

(Watts of Power at Detector)

The computed signal levels were then used to anticipate what signal ranges would be encountered in the instrument, so that the individual detector gains could be set. Analysis of published data suggested that we might encounter relatively narrow distributions, so the gains were chosen to accomodate the maximum loading (40 parts per billion) in any one channel. A preference was expressed for gains that were simply related to one another, to facilitate computations and calibration.

The relative gains are listed in Table 11, column 2. These gains were set by adjusting feedback resistors, and the experimentally measured values are given in columns 3 and 4.

Table 11: Detector Gains

Angle	Selected Gain	Experimentally Determined	
		Red	Blue
3.9°	4	4.47	4.29
7.8°	2	2.34	2.184
11°	2	2.34	2.046
$90°P_1$	40	40.00	40.00
$90°P_2$	40	42.88	40.87

The next step involved adjusting the scattering equations for the various gain, transmission, and common volume differences. Then it was necessary to correct each volume response equation to produce the same signal for unit loading at its peak region. The results are summarized in Table 12.

Table 12: Preliminary Channel Equations

Channel (Size)	Multiplier x Formula
A (.2)	2.143 x (1.0 (41) - 0.8 (42)) / (46)
B (.4)	4.89 x (1.0 (91) - 0.8 (92)) / (96)
C (1.)	6.013 x (1.0 (93) - 0.3686 (94) + 0.0317 (95)) / (96)
D (3.)	5.56 x (0.3519 (43) - 0.7832 (44) + 1.0 (45)) / (46)
E (7.)	9.168 x (0.3739 (93) - 0.8387 (94) + 1.0 (95)) / (96)

The circled values represent signals from the respective colors and detectors, including gains. No correction is needed for relative spectral sensitivity of the detectors, since the ratio removes spectrally induced gain differences.

MATRIX DECOUPLING

There is some spillover of response between adjacent channels, and to reduce this problem, a matrix decoupling is applied. The spillover is computed by normalizing the response functions into five equal log interval regions. This produced a five by five matrix of values. The inverse of this matrix provides the sequence of numbers to unfold a more accurate distribution from the measured one. The coupling matrix and its inverse are shown in Table 13. This decoupling is applied after the individual channel

signals, C_i, are measured. The final histogram components are designated as H_1 through H_5.

INVERSION OF A MATRIX WITH 5 VARIABLES					NORMALIZED RESPONSE FOR
1.0000	.0130	.0310	.0210	.0000	0.2 (Microns)
.3380	1.0000	-.0650	-.0620	.0070	0.4
.0125	.2740	1.0000	.1090	.0580	1.0
.0000	.0040	.1760	1.0000	.0590	3.0
.0000	-.0020	.0250	.4830	1.0000	7.0

THIS IS THE INVERSE OF THE MATRIX

1.0021	-.0053	-.0280	-.0197	.0028
-.3343	.9868	.0628	.0684	-.0146
.0803	-.2745	.9991	-.1035	-.0499
-.0130	.0451	-.1798	1.0476	-.0517
.0036	-.0130	.0620	-.5033	1.0262

$$\times \begin{bmatrix} C_1 \\ C_2 \\ C_3 \\ C_4 \\ C_5 \end{bmatrix} = \begin{bmatrix} H_1 \\ H_2 \\ H_3 \\ H_4 \\ H_5 \end{bmatrix}$$

Table 13: Normalized Response for Each Zone and the Inverse Matrix Used for Decoupling.

IN-HOUSE CALIBRATION OF THE COMPLETED UNIT

Calibration of the finished unit was complicated by several factors. The most difficult portion was obtaining a sample material covering the size range of interest that was sufficiently well characterized to be used as a reference standard. Several iterations were made before coming to a satisfactory material and set of instrumental constants which gave consistent results.

Initially, attempts were made to use suspensions of diamond dust in water. A specially designed cuvette, 35 cm long and 2.5 cm wide was built to hold the suspension, and a significant amount of effort was put into sizing the diamond dust distributions using electron microscopy.

However, there are some optical difficulties involved with liqud suspensions that had not been recognized until the actual testing began. During the measurements, two artifacts of the cuvette system were discovered.

1. The longer wavelength (0.9 microns) is severely attenuated by the path through water. Approximately 90% of the light is lost in each of the three forward channels to absorption by the water. Accordingly, all forward measurements at this wavelength appeared initially to be only 10% of expected value.

2. The refraction that occurs at the air/glass/water interface is accentuated by the off-axis position of the forward scattering system, as illustrated in Figure 25. Refraction changes the effective common volumes, slightly increasing the observed volume in the 11 and 7.8 degree channels, and substantially reducing the illuminated volume observed by the 3.9 degree channel. These effects may be color dependent, since beam cross-section is not identical in both colors.

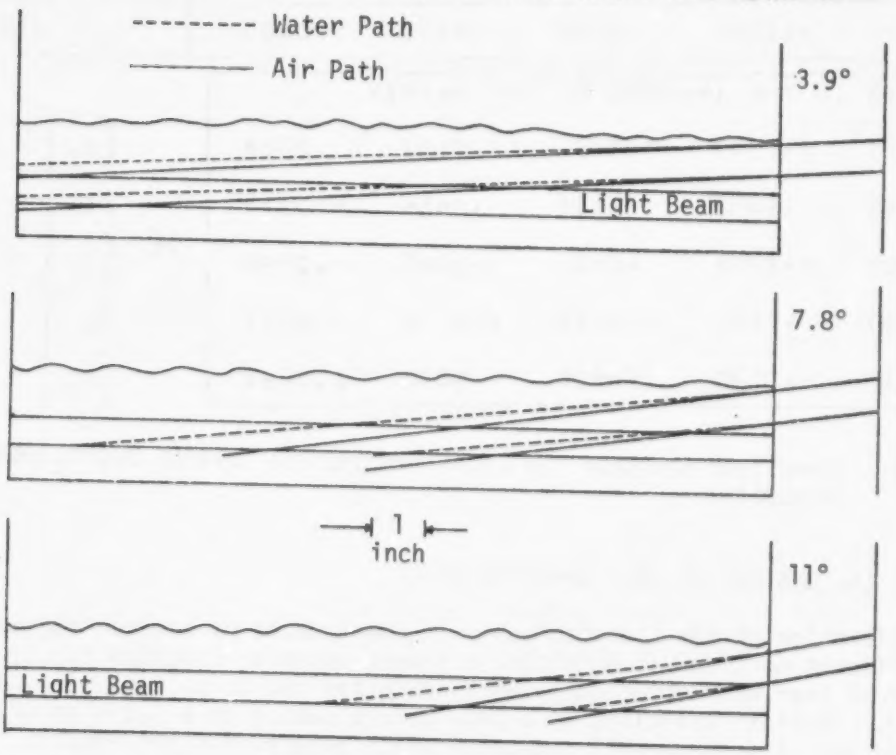

Figure 25: Comparison of Forward Scattering Common Volumes with and Without Water in Cell

In addition to diamond dust, polystyrene spheres in two size ranges, 1.1 microns and 5.7 microns were evaluated in liquid suspension. The results of the diamond and polystyrene tests were consistent with the artifacts defined above, but it was not possible to correlate them with theory

without doing extensive additional testing. The use of water suspended material was then abandoned in favor of aerosol suspensions, consistent with the intended use in the stack.

The aerosol experiments were performed to determine the combined effect of detector gain, fiber transmission, common intercepted sample volume, and aperture size for each of the forward scattering channels, and to verify the balance between red and blue signals.

Considerable thought went into the choice of a proper aerosol. For particles larger than 1 micron, the Mie scattering properties show resonances, and accurate determination of particle size to within a few tenths of a micron is essential. In addition, the refractive index of the material effects the resonances. The index should be known to within 0.01 for accurate analysis of the data if monodisperse particles are used for calibration.

The absolute index and the particle size are much less critical for scattering material in the Rayleigh region. Strictly, this is on the order of 0.1 micron or smaller, but in practice, the transition region between Rayleigh and Mie scattering allows some flexibility in the upper size limit of a broad sub-micron aerosol used for calibration, as will be discussed.

Rayleigh scatterers are desirable for these experiments, since the ratio of any two forward scattering signals is independent of diameter. Therefore, the actual particle size distribution need not be known when all the particles are in the Rayleigh region. Figures 26 and 27 show the forward scattering signals vs. diameter for small particles at wavelengths .45μ and .90μ, respectively. The region of constant slope is characteristic of Rayleigh scattering. The upper limit is not well defined but occurs for diameters of approximately 0.4μ and 0.8μ, respectively. Below this size the ratios of any two forward scattering signals are identical at both wavelengths. This is a convenient method of determining if an aerosol meets Rayleigh scattering criteria.

Four different sources of small particles were investigated; the Phoenix aerosol generator, cigar smoke, ammonium chloride smoke, and cigarette smoke. The distribution of the Phoenix generagor is specified by the supplier to be 92% below 1μ. This distribution can be shifted to smaller diameter by diluting the aerosol source material, DOP, with isopropyl alcohol. The alcohol in each primary droplet evaporates, leaving a DOP droplet of reduced size. For example, a 1% solution of DOP in isopropyl is expected to reduce the particle size by a factor of 0.215. One percent and 0.5 percent solutions were used in the experiments.

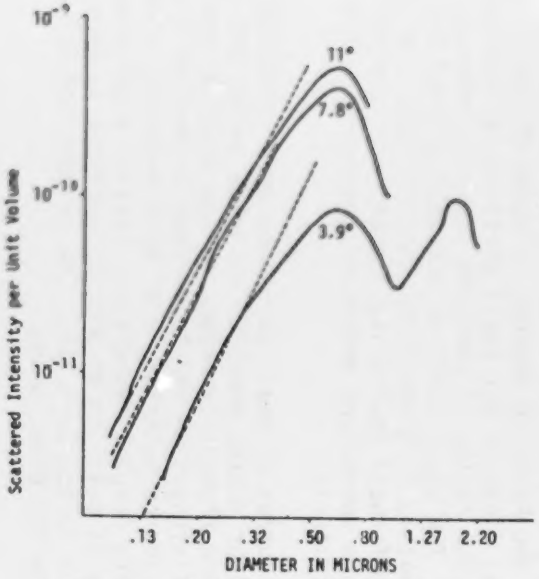

Figure 26: Flux/Unit Volume vs. Particle Diameter for DOP, Aerosols, λ = 0.45 microns

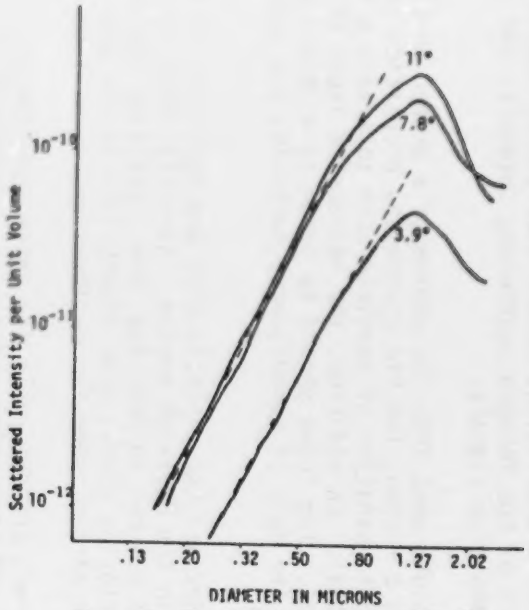

Figure 27: Flux/Unit Volume vs. Particle Size for DOP, Aerosols, λ = 0.09

Cigarette smoke has been measured by many people using different techniques. Most references place the size well below one micron, and one recent article defines the mass mean diameter of total particulate matter in the 0.5 to 0.75 micron range[7] (filtered cigarette). Ultimately, cigarette smoke was found to contain the smallest size particles, and was used as the technique for calibrating the forward scattering channels. Cigar smoke was also tried, but subsequently determined to be bimodal.

The system used in the laboratory to produce the smoke aerosols is shown in Figure 28. A filtered cigarette was connected to the inlet of a 1 cfm diaphragm pump. The output of the pump filled a 2.4 cubic foot mixing chamber before entering the probe sample region, to promote homogeneous aerosol concentration throughout the probe. The purge system could not be used at such low flow rates. Therefore, microscope slides were placed over the 90° apertures and at each end of the slot to contain the aerosol to the sampling region. The same procedure was used with the Phoenix aerosol except that the flow was powered by a compressed nitrogen tank.

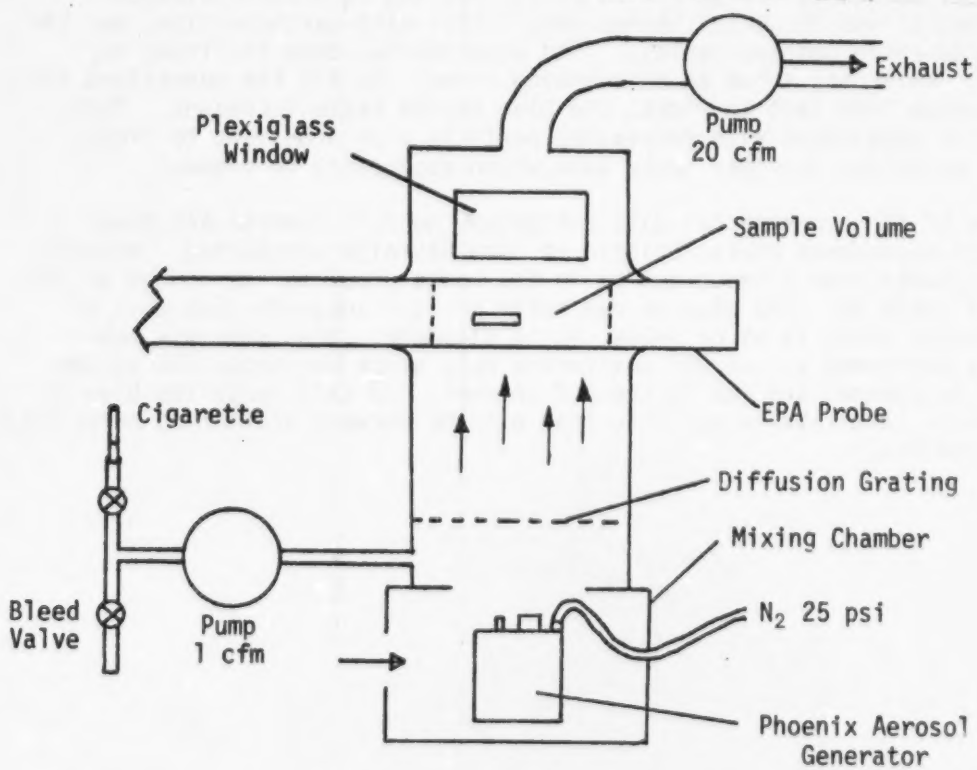

Figure 28: Laboratory Sample System for Delivery of Aerosol Smokes

Data on all three samples was taken at various smoke concentrations testing for multiple scattering by checking whether all angular scattering signals increased by the same percentage as the loading increased. No multiple scattering was detected.

Uniform sample flow was very important, since each of the three forward angles intercepts a different volume of material in the sample region. During the experimentation, a plastic window was inserted on the exit side of the sample chamber, after the probe, to permit visual inspection of the material flowing through the sample slot. Occasional turbulence and non-uniformities in flow were observed, and the sample flow system was changed to eliminate those problems.

The 7^{o} and 3^{o} signals were divided by the 11^{o} signal in each of two colors to cancel the effect of particle loading. Comparisons to theory were then made on the basis of these ratios. Then, since true Rayleigh scattering scales as inverse 4th power with wavelength, the ratio of blue to red at any low forward angle indicates the extent of Rayleigh scattering. The ratio at 11^{o} was used throughout. These five parameters are compared in Tables 14 and 15. Table 14 lists the results predicted by the preliminary theoretical constants for particles of .1, .4, and .5 microns diameter. Notice that 3^{o} and 7^{o} ratios change very little with particle size, but the blue to red ratio changes rapidly. The experimental data is listed in Table 15. This data shows an interesting trend. As all the normalized signals decrease from left to right, the blue to red ratio increases. This behavior is consistant with decreasing particle size from left to right. The only exception is cigar smoke data which appears to be bimodal.

None of the experimental data exhibited the full inverse 4th power wavelength dependence characteristic of pure Rayleigh scattering. However, cigarette smoke came closest and is in the range predicted by values at the bottom of Table 14. The blue to red ratio of 11.4 suggests that most of the cigarette smoke is at or below .5μ in diameter. This size was subsequently confirmed by the 90^{o} scattering data which indicated 85% volume in the 0.4μ channel and 15% in the 0.2 channel. In this range the blue to red ratio is sensitive to particle size but the forward scattering normalized signals are not.

Table 14: Theoretically Predicted Ratios for Three Particle Sizes

	Size (Microns)		
	0.1	0.4	0.5
λ = .45μ			
7°/11°	1.100	1.133	1.202
3°/11°	.491	.517	.544
λ = .90μ			
7°/11°	1.063	1.069	1.105
3°/11°	.507	.511	.514
Blue/Red 11°	20.	15.	10.2

Table 15: Experimental Data with Various Aerosols

	Cigar	1% DOP	0.5% DOP	Cigarette	Cigarette Data at 0.5 microns: Theoretical/Experiment
λ = .45μ					
7°/11°	1.058	1.033	.966	.914	1.315
3°/11°	.558	.412	.405	.315	1.727
λ = .90					
7°/11°	.979	1.142	1.102	.940	1.175
3°/11°	.398	.541	.418	.306	1.680
Blue/Red 11°	1.99	4.27	5.08	11.4	

Table 16: Final Constants for the Prototype, as Built.
The matrix (Table 13) remains unchanged.

$$C_1 = .605\ (\textcircled{41} - .7462\ \textcircled{42})/\textcircled{46}$$

$$C_2 = .520\ (\textcircled{91} - .7830\ \textcircled{92})/\textcircled{96}$$

$$C_3 = .639\ (1.0\ \textcircled{93} - .4331\ \textcircled{94} + .0533\ \textcircled{95})/\textcircled{96}$$

$$C_4 = 1.570\ (0.3619\ \textcircled{43} - 1.030\ \textcircled{44} + 1.727\ \textcircled{45})/\textcircled{46}$$

$$C_5 = .974\ (0.3739\ \textcircled{93} - 0.9855\ \textcircled{94} + 1.680\ \textcircled{95})/\textcircled{96}$$

Therefore, by comparing the 0.5μ theory and experimental cigarette data, as shown in Table 15, corrections to the original equations can be made, corresponding to the performance of the instrument as built. The five forward scattering equations are listed in Table 16.

Figures 29 and 30 present instrumental measurements on materials made during the final calibration. Figure 29 shows cigarette smoke runs at several different concentrations. This was the only material investigated that consistently showed all sub-micron particles. Separate experiments were performed with a combination of ammonia and hydrochloric acid fumes, which combined to form a white cloud of ammonium chloride smoke. Although reported to be submicron material under ideal conditions, agglomeration is claimed to be a problem, and this seemed to be the case for our samples as prepared in the test system. Two different arrangements of the sample presentation were attempted.

Figure 30 shows the progression of the increase in size with changing concentration in a combination of di-octyl phthalate (DOP) and alcohol. There is occasionally a small amount of material shown in the largest size channel, which may be artifact of the system, or may represent a truly bimodal distribution.

The bimodal nature of at least one material, cigar smoke, was confirmed by separate analysis of the scattering data. Measured data is shown at the bottom of Figure 30.

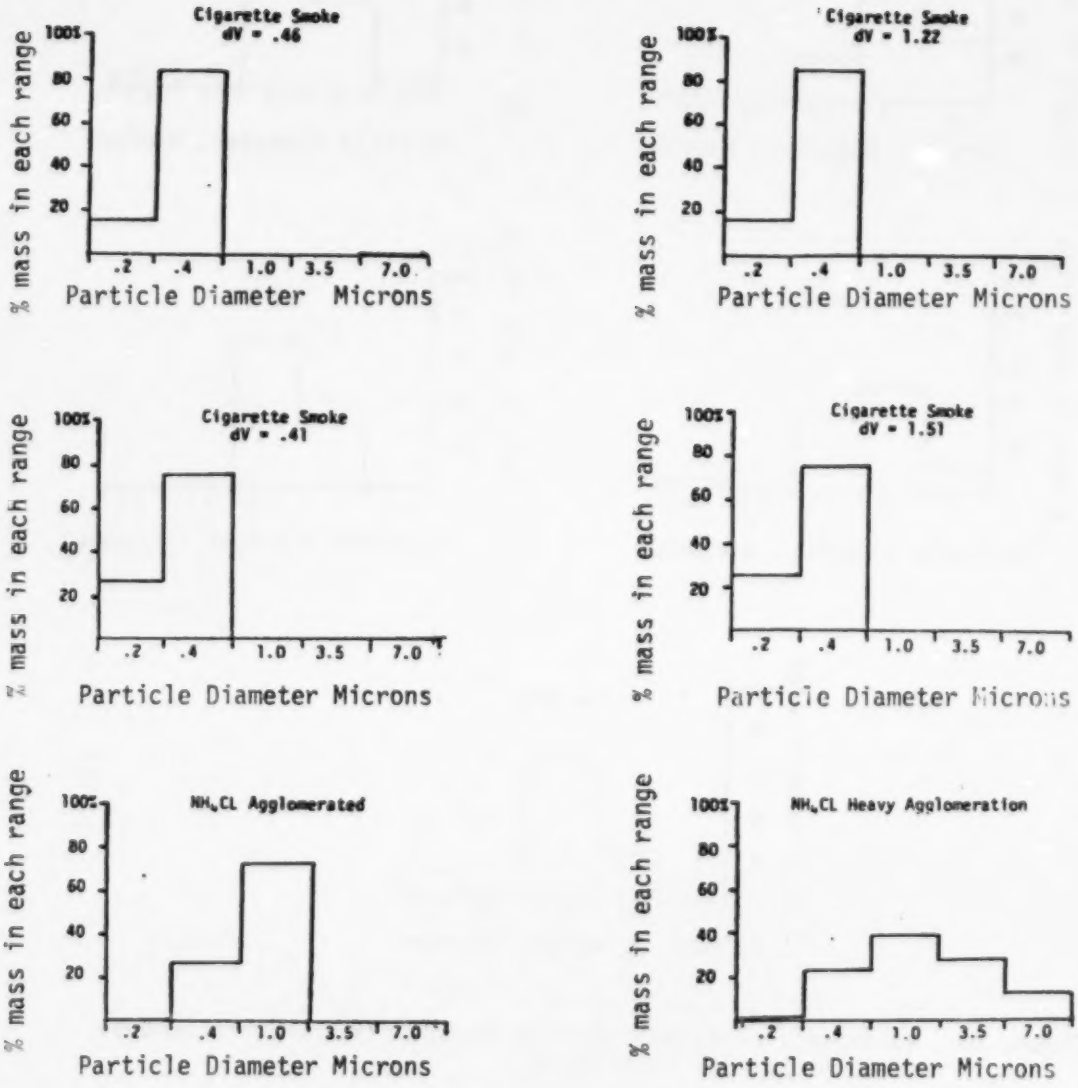

Figure 29: Volumetric Histograms of Several Smokes

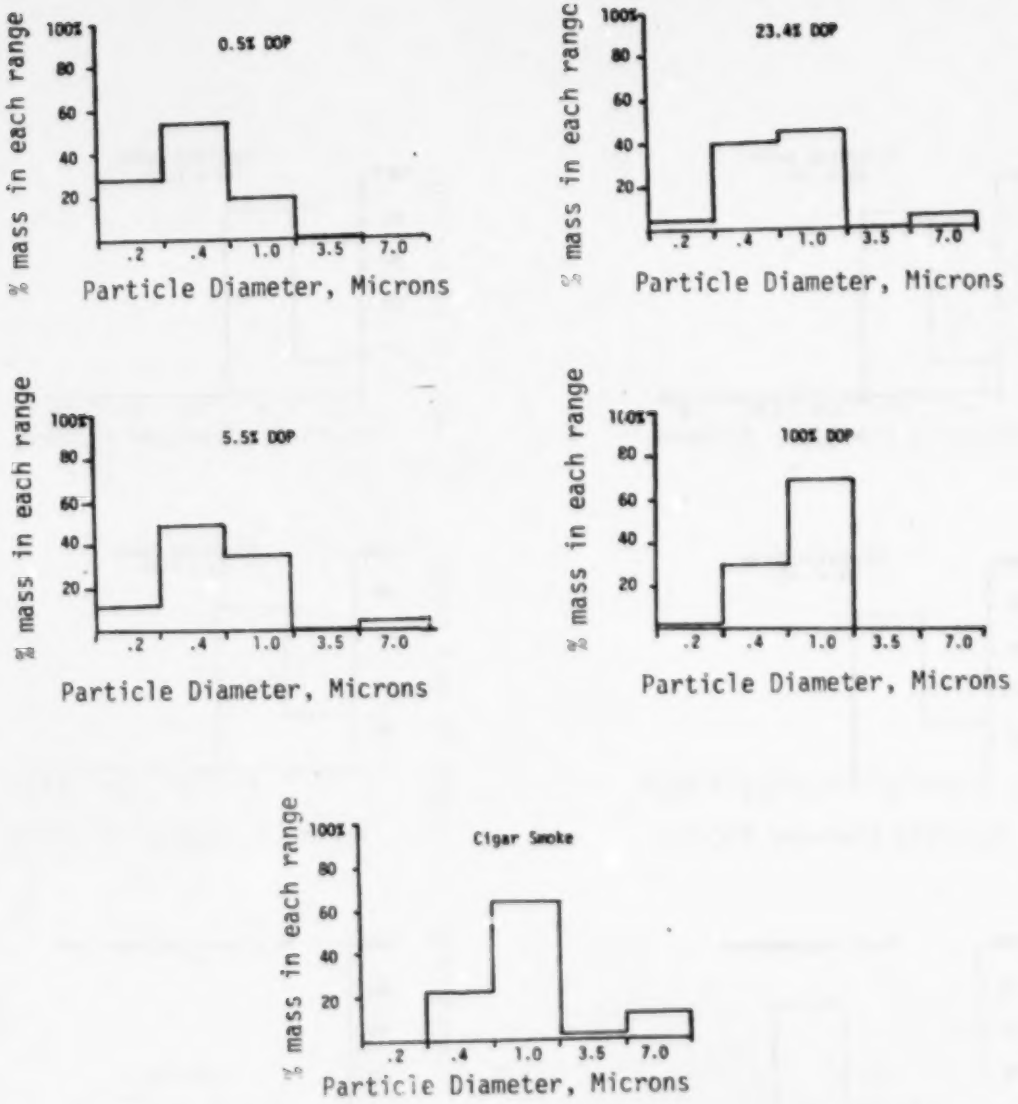

Figure 30: Volumetric Histograms for Various Dioctylphthalate Concentrations and for Cigar Smoke.

FIELD TRIAL AT EPA FACILITY

During the period of May 15 through 19, 1978, ten experiments were performed at an EPA source simulator facility in North Carolina. Three different size distributions of fly ash were measured in the simulator. The simulator is a closed loop wind tunnel with accompanying subsystems to simulate source emissions. Particulate emissions are simulated by dispersing powders into the tunnel with a fluidized bed particulate generator. A complete description of the simulator and particulate generator is given in reference 8. Size distribution data was recorded with the stack emissions monitor and a seven stage cascade impactor. The impactor was located 5.5 feet up stream from the monitor. Tunnel flow was maintained at 35 ft/sec for all runs.

Each sample of fly ash was measured three times, a total of nine runs. The tenth run, which lasted one hour, tested the integrity of the purge system for long term measurements. Table 17 lists the fly ash sample number, span, sample time and duration of each experiment. The span indicates full scale in parts per billion; it is inversely porportional to gain. The sample time is the total measurement time for each of two wavelengths. The total time between data printouts is twice the measurement time.

Raw data from the scattering signals was collected, but technical difficulties with the microprocessor constants prevented on-the-spot calculations of the size distribution. Many sets of optical scattering data were taken for each impactor run, and transmissometer readings were made continuously during the tests.

The amplitudes of the raw data from the optical scattering measurements tracked very well with the transmissometer data, rising and falling together, as the loading varied during each test. Only one impactor sample was collected per run, representing the average over the entire period.

After the final calibration was complete, the raw data sets from optical scattering were processed by computer as they would have been with the associated digital microprocessor. To compare the optically generated signals to the distribution measured by the impactor, some manipulation of the impactor data was required. It was corrected for a density of 2.3 gm/cm^3, typical of fly ash, and graphed on a cumulative distribution plot.

Table 17: Fly Ash Sample Tests at EPA-RTP Source Simulator - May, 1978

Test Number	Fly Ash Sample Number	Span (ppb)	Sample Time (sec)	Date and Duration of Test	Number of Light Scattering Data Sets Taken
1	1	100	64	5/17/78 * 9:48 - 10:18	11
2	1	100	64	5/17/78 1:15 - 1:55	17
3	1	40	64	5/17/78 2:35 - 2:55	**
4	2	100	64	5/18/78 9:37 - 9:57	9
5	2	40	64	5/18/78 11:02 - 11:27	**
6	2	100	64	5/18/78 1:10 - 1:25	7
7	3	100	64	5/18/78 2:05 - 2:20	7
8	3	100	64	5/18/78 3:00 - 3:10	4
9	3	100	64	5/18/78 3:40 - 3:50	4
10	3	100	128	5/18/78 3:50 - 5:00	No Data Taken

* Run made without glass beads in the fluidized bed particulate generator.

** Overrange conditions at one wavelength prevented acquisition of complete data.

Next, channel edges, corresponding to those listed in Table 4, were identified and the mass was read in each of the five size regions measured by the scattering instrument. Finally, the histogram of the impactor measured mass distribution was computed by normalizing by the total mass in the size range of 0.11 to 13.3 microns.

Graphs of five runs represent different size distributions used in the testing are presented in Figure 31. The scattering data is shown as the solid line histogram, and the impactor data is indicated by the dashed lines and circles. Only one set of scattering data is graphed for each run, but the size variations in most cases were minimal. The optical data indicates that most of the material is in the range of 1 micron or greater, while the impactor usually defines a distribution with a more well defined peak but a tail extending over a broader range. Table 18 contains the numerical results as graphed in Figure 31.

Difference between impactor and optical data as shown may be due to the following things:

1. The two measurement techniques define boundaries for size fractions in different manners.

2. The reduction of impactor data to optical scattering channels introduces some errors.

3. The raw data printed out in 3 digit format and used in computer processed optical data is not as accurate as that available to the actual microprocessor. A 10% error in raw data for channels 1 and 4 (0.2 microns and 3.5 microns) is possible.

4. The sample collection procedure for the impactors showed different results from the free stream state of the material. This is evident in at least one case, runs 1 and 2, where the sample in the free stream was consistently measured differently for the two runs, while the impactor data showed them both very similar. Large glass beads were added to the sample conditioner hopper for the second and subsequent runs, and this appears to have changed the characteristics of the air entrained material between otherwise identical runs one and two.

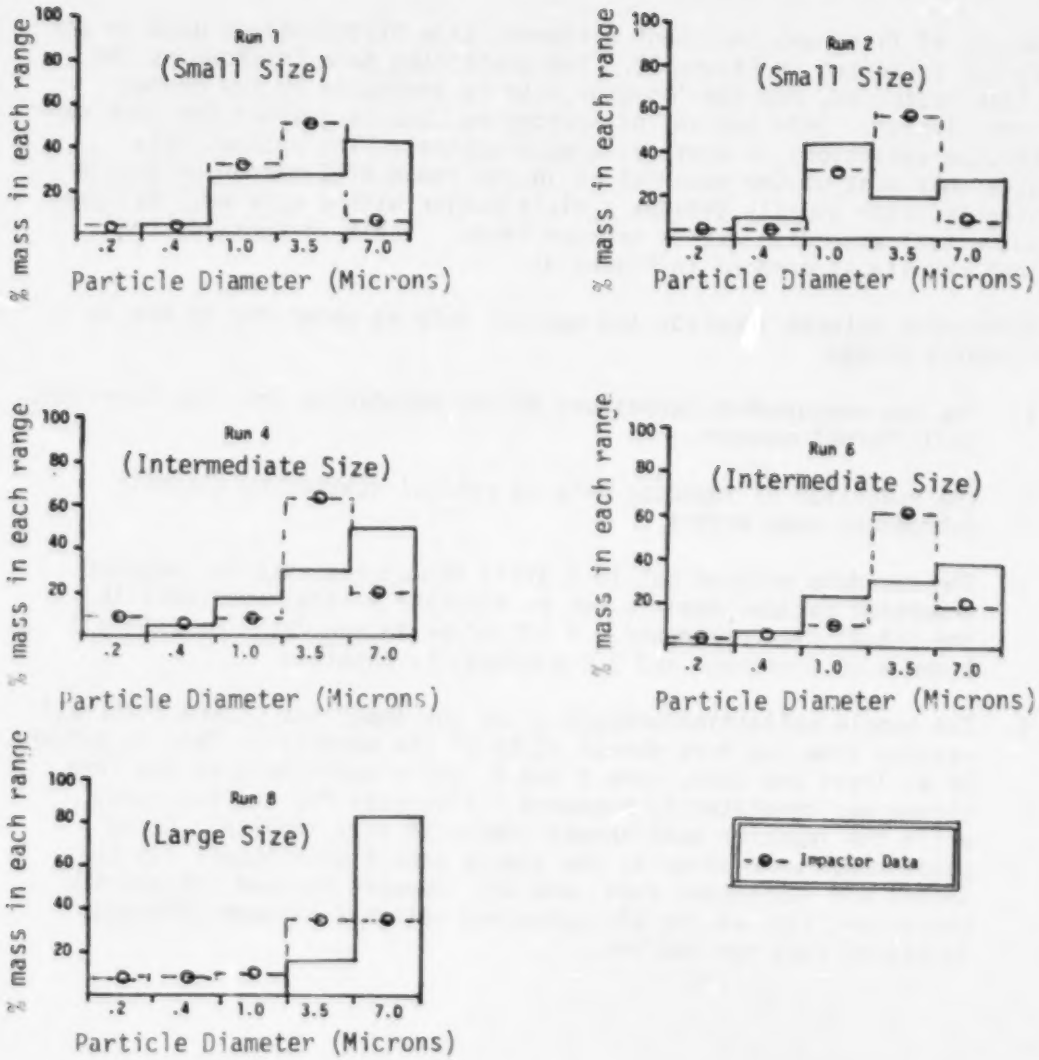

Figure 31: Size of Fly Ash as Measured by Impactor and Optical Monitor at EPA, RTP Source Simulator.

Table 18: Impactor and Optical Volume Histograms for May, 1978 EPA/RTP Tests

Channel Center Particle Diameter, μm		Impactor Run Number				
		1	2	4	6	8
Center	Width					
0.2	0.14 to 0.30	3.6%	3.2%	4.9%	3.8%	7.0%
0.4	0.30 to 0.75	2.9	3.7	3.0	4.9	10.2
1.0	0.75 to 2.0	31.8	31.0	9.0	10.0	12.5
3.5	2.0 to 5.0	54.5	54.7	63.7	62.0	35.9
7.0	5.0 to 13.3	7.2	7.4	19.4	18.0	34.4
		Optical Data Run				
		1•5	2•5	4•5	6•5	8•2
0.2	0.14 to 0.30	0%	0%	0%	0%	0%
0.4	0.30 to 0.75	5.5	9.3	5.2	6.4	1.3
1.0	0.75 to 2.0	26.3	43.1	16.3	23.1	0
3.5	2.0 to 5.0	26.0	19.6	29.4	31.3	16.4
7.0	5.0 to 13.3	42.2	28.0	49.1	39.2	82.4

FIELD TRIAL AT A COAL-FIRED FACILITY

On June 27 and 28, 1978, the prototype on-stack instrument was tested at an East Coast coal fired power plant. Optical data was to be taken from a 15,600 m^3/min horizontal flow duct, which led directly to the base of a stack. In addition, Ray Steward of EPA and Bruce McElhoe of Northrop Services (subcontractors to the EPA), took data with an eight-stage cascade impactor. The tests were designed to determine the reliability, ease of use, and performance of the probe under actual field conditions.

The week before the test we went to the site to clear out the two test ports (one for the impactor and one for the prototype probe) and to build a wooden deck to serve as a work platform during the tests. The test site was outside, along the horizontal run of the duct, accessible by a catwalk. The ports were difficult to clear and the positive pressure and sulfuric acid fumes made this a very unpleasant task.

The instrument was set up on Tuesday morning, June 27. The xenon lamp required several starts before it fired, but the high humidity that date may have caused this. Vibration of the stack and the platform caused the focus of the lamp to oscillate one half inch laterally in the pinhole plane and final adjustment was difficult. The amount of beam misalignment was not reproducible when the transceiver cover was attached. The system was finally aligned through trial and error and varying tension on the cover. Steps were later taken to correct this problem by adding adjustment access ports to the cover, so that final adjustments are now made with the cover on.

The stack flow was measured at 5.5 m/sec and the stack temperature was 154°C. The impactor was inserted and we made a four minute measurement. Then the probe was pulled out and allowed to cool for window inspection. Both 90° windows were clean, but the forward window had a thin layer of fly ash. This layer did not cause appreciable optical attenuation.

The windows were cleaned and the lamp was restarted. The system was aligned and probe inserted into the stack with the blower at a (dial indicated) head pressure of 127 cm. This pressure was maintained while waiting for the impactor, to avoid any fouling of the forward window. After five minutes the blower shut off due to thermal overload; the high pressure had caused the motor to overheat. Operating instructions now indicate the proper operating pressures to avoid this problem. After the purge shut off, the windows were exposed to flyash, and the probe was withdrawn from the stack to clean the windows. The forward window showed the same amount of dirt as when the purge system was operating. In later discussions with a consultant in flow dynamics we decided that the fouling occurs during insertion, when the positive pressure forces dirt laden air in through the beam exit hole, near the forward windows. Purge operation during normal running conditions seems satisfactory.

The windows were cleaned and new background readings taken. The probe was inserted in the port and measurements were recorded during two consecu-

tive impactor runs. The blower was run at a head pressure of 68.6 cm to avoid fouling of the forward window. After these two tests, more data was taken at a reduced head pressure of 43.2 cm to see the effect of the purge on the common volumes. Table 19 summarizes all the test conditions.

Table 19: Test Conditions

Test Number	Impactor Number	Span	Function	Sample Time (Sec.)	Head Pressure	Duration
1	1	400	1	64	48.3 cm	12:20-12:25
2	2	400	3	16	68.6 cm	4:47-4:52
3	3	400	3	16	68.6 cm	5:00-5:03
4	--	400	3	16 and 32	43.2 cm	5:09-5:19

A summary of the impactor data, adjusted as described earlier to fit the optical instrument channels, is included in Table 20. The corresponding optical data is shown below the impactor runs.

In these tests, there was a great disparity between optical and impactor readings, with the prototype indicating approximately 87% of the material in the largest size fraction while the impactor data shows a broader distribution, peaked at 3.5 microns. No single factor explains the difference but several observations were made at the site.

1. The loading was extremely high,

2. Some re-entrainment of fly ash was occuring from the collection hoppers,

3. There was considerable turbulence and flow variation in the region of measurement, and

4. The impactor and the optical probe were inserted in separate ports, several feet apart.

The optical instrument was working properly before and after the test, so we feel that the scattering data is accurate. However, the discrepancies were larger than anticipated, based on the RTP tests in May, 1978. The major interest in performing this test was to gain practical experience with the instrument in that environment, and that goal was accomplished.

Table 20: Field Test Data from Coal Fired Facility

Impactor Data (Microns)	Run 1	Run 2	Run 3
0.2	3.4%	2.25%	1.14%
0.4	5.9	4.5	4.09
1.0	15.7	18.3	15.2
3.5	38.6	45.0	43.2
7.0	36.4	30.0	36.4
Optical Data			
0.2	0.0%	0.0%	0.0%
0.4	2.2	2.5	2.6
1.0	3.5	5.6	5.9
3.5	7.3	4.4	4.2
7.0	87.3	87.5	87.3

MODIFICATIONS DURING SYSTEM TESTING

During calibration and testing, a number of modifications and changes were made to various parts of the system. The most significant ones are described here.

1. A large random drift of the electrical background was discovered and corrected. The cause was traced to high frequency electrical noise at the ADC input, which was successfully eliminated with the addition of a capacitor filter. Additional stability was added by installing a lower resistance ground cable for the 50 foot connection between the lamp housing on the probe and the digital microprocessor ccbinet. Backgrounds are now stable to within one or two counts.

   Other work involved elimination of unstable offset signals from the ADC. These signals had a dependence on gain setting due to a small tuning error. More careful tuning of the analog circuitry and addition of a positive overrange trap eliminated spurious signals when excessive scatter signals are present.

2. A high level of optical background in the 3.9° channel at 0.9 microns was traced to specular reflection in the interior of the probe sheath. It was found that infrared illumination was being scattered from dirt on the collimating lens and then reflected from the sheath wall into view of that detector. This problem was solved by proper sizing and location of intermediate baffles inside the probe sheath. However, it is important that cleanliness of the lens be maintained even though small deposits of dust no longer drastically change the background.

   In addition to final adjustment of the anti-reflection baffles, an enclosure was installed around the chopper and filter assembly. This was done to eliminate stray light from this part of the system being reflected into the detector region.

3. During field trial testing, the main beam monitor showed excessive sensitivity to alignment. Realignment after shipping produced different relationships between beam strength and ADC counts, which resulted in changes in calibration of the system. This problem was solved by removing the fiber optic line and placing the silicon detector at the focus of the reflected reference beam. This change produced a much more stable beam strength signal, free from variations due to realignment or residual flexing of the probe. The entire focused spot, rather than a portion of the beam, now falls on the detector.

4. There were several problems relating to the xenon lamp and power supply. During testing, one of the two power transistors shorted. Both were replaced with higher rated transistors. Additionally, a plexiglass window was installed in the xenon power supply box so the voltage and current meters could be monitored during the operation of the lamp.

5. Arcing to the chassis was a problem when starting the lamp, so the lamp housing was isolated from the chassis by adding a Delrin plate. Additional electrical wiring changes were made to reduce the induced current during the starting pulse. The lamp electrical power now comes directly from the line cord to the power supply and the starting controls were moved to the lamp power supply from the control console. These and other associated changes were sufficient to significantly reduce the arcing difficulties.

SECTION 6

CONCLUSIONS

Optical techniques involving low angle forward and polarization dependent 90° scattering have been combined in an instrument package for real time particulate sizing in stationary sources. An insertable probe was fabricated, designed, and engineered for use in high temperature acid environments. Associated equipment, such as an air purge system and sophisticated electronics detection and microprocessor package, was designed and constructed.

The response per unit volume of material for each of the five channels is shown in Figure 32.

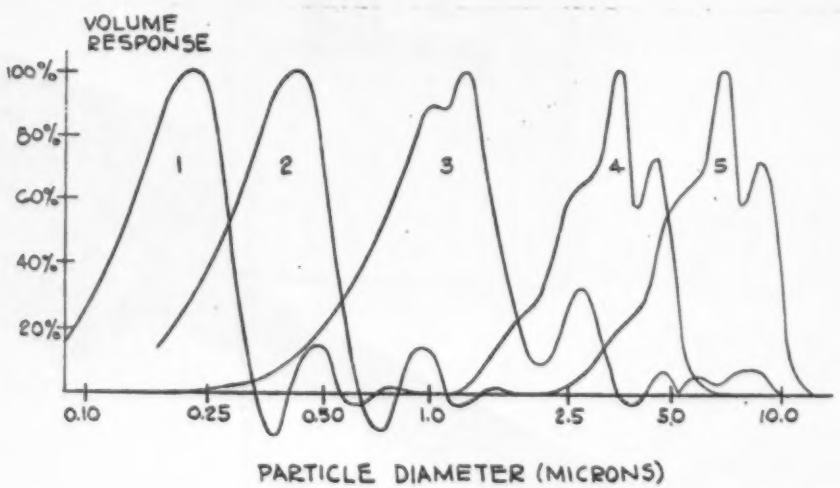

Figure 32: Volumetric response curves, as a function of particle diameter, for the five channels of the prototype. Curves 1 and 2 are obtained with 90° scattering, and curves 3, 4, and 5 from forward scattering. These curves are for silica, with refractive index of 1.5.

A photograph of the completed prototype is included as Figure 33, and the operational characteristics of the unit are defined in Table 21. The instrument offers a method for in-stack analysis of particulate size without dilution or extraction of material, and directly produces a distribution of the particulates by volume fraction. This device thus provides a unique and valuable measurement capability for analysis and monitoring of particulates in source emissions.

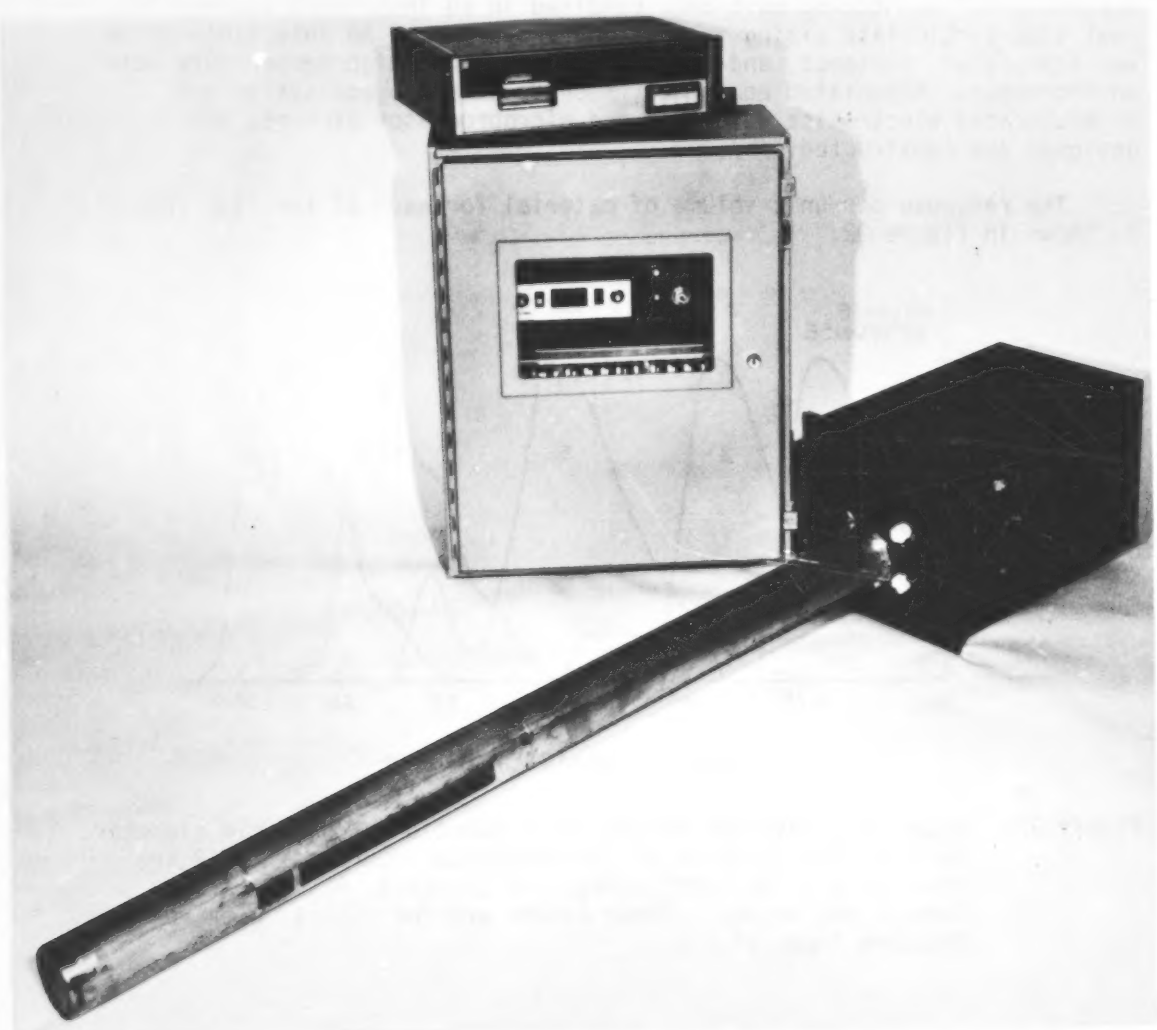

Figure 33: Probe, electronics package, and digital printer used for measuring the size of particulate material in utility stacks.

Table 21: Characteristics of Prototype Light Scattering Instrument

Size Range (Particle Diameter)	0.1 to 10.0 microns
Size Discrimination	Five volume fractions with centers at 0.2, 0.4, 1.0, 3.5, and 7.0 microns
Anticipated Loading Range	0.01 to 0.1 grams of material/meter^3 or 4 to 40 parts/billion by volume (with s.g. of 2.5)
Operational Range	4 to 400 parts/billion
Mode of Operation	Low angle forward scattering and 90° polarization dependent scattering
Power Requirements	115 volts, 60 Hz, 2 20 amp outlets
Operational Temperature	Probe portion in stack: up to 260°C (500°F)
	Transceiver portion and other electronics outside stack: 0° to 43°C (32° to 110°F)
Speed of Measurement Sequence (Acquisition of Data)	Integration time selectable from 4 to 256 seconds

REFERENCES

1. Mie, G., Beitrage Zur Optik truber Medien. Annalen Der Physik, 3: 377-445, 1908.

2. Kerker, M., The Scattering of Light and Other Electromagnetic Radiation. Academic Press, New York, 1969. 666 pp.

3. Van de Hulst, H.C., Light Scattering by Small Particles. John Wiley & Sons, New York, 1957. 470 pp.

4. National Bureau of Standards. Tables of Scattering Functions for Spherical Particles. Applied Mathematics Series - 4. U.S. Gov't Printing Office, Washington, 1948. 119 pp.

5. Dave, J.V., Subroutines for Computing the Parameters of the Electromagnetic Radiation Scattered by a Spheres. Report No. 320-3237. IBM Scientific Center, Palo Alto, CA, 1968. 65 pp.

6. Fisher, G.L., et. al., Physical and Morphological Studies of Size-Classified Coal Fly Ash. Environmental Science and Technology. 12(4): 447-451, 1978.

7. Morie, G.P., and M.S. Baggett. Observations on the Distribution of Certain Tobacco Smoke Components with Respect to Particle Size. Beitrage Zur Tabakforschung. 9(2): 72-78, 1977.

8. Moran, M.J., Simulated Stationary Source Facility Users Handbook. TN-262-1535, Northrop Services, Inc., Huntsville, AL, October 1975.